Pre-existing normal faults have limited control on the rift geometry of the northern North Sea

Johan S. Claringbould[1]*, Rebecca E. Bell[1], Christopher A-L. Jackson[1], Robert L. Gawthorpe[2], Tore Odinsen[3]

[1]Basins Research Group (BRG), Department of Earth Science and Engineering, Imperial College, London, SW7 2BP, UK
[2]Department of Earth Science, University of Bergen, Allégaten 41, 5007 Bergen, Norway
[3]Statoil ASA, Sandslihaugen 30, 5254 Sandsli, Norway

**Corresponding author: Earthquake Research Institute, The University of Tokyo, 1-1-1 Yayoi, Bunkyo-ku, Tokyo, 113-0032, Japan.*
Email address: jsclaring@eri.u-tokyo.ac.jp

Abstract

Many rifts develop in response to multiphase extension with numerical and physical models suggesting that reactivation of first-phase normal faults and rift-related variations in bulk crustal rheology control the evolution and final geometry of subsequent rifts. However, many natural multiphase rifts are deeply buried and thus poorly exposed in the field and poorly imaged in seismic reflection data, making it difficult to test these models. Here we integrate recent 3D seismic reflection and borehole data across the entire East Shetland Basin, northern North Sea, to constrain the long-term, regional development of this multiphase rift. We document the following key stages of basin development: (i) pre-Triassic to earliest Triassic development of multiple sub-basins controlled by widely distributed, NNW- to NE-trending, east- and west-dipping faults; (ii) Triassic activity on a single major, NE-trending, west-dipping fault located near the basins western margin, and formation a large half-graben; and (iii) Jurassic development of a large, E-dipping, N- to NE-trending half-graben near the eastern margin of the basin, which was associated with rift narrowing and strain focusing in the Viking Graben. In contrast to previous studies, which argue for two discrete periods of rifting during the Permian-Triassic and Late Jurassic-Early Cretaceous, we find that rifting in the East Shetland Basin was protracted from pre-Triassic to Cretaceous. We find that, during the Jurassic, most pre-Jurassic normal faults were buried and in some cases cross-cut by newly formed faults, with only a few being reactivated. Previously developed faults thus had only a limited control on the evolution and geometry of the later rift. We instead argue that strain migration and rift narrowing was linked to the evolving thermal state of the lithosphere, an interpretation supporting the predictions of lithosphere-scale numerical models. Our study indicates that additional regional studies of natural rifts are required to test and refine the predictions of physical and numerical models, more specifically, our study suggests models not explicitly recognising or including thermal or rheological effects might over emphasise the role of discrete pre-existing rift structures such as normal faults.

Keywords: multiphase rift, pre-existing fault, fault reactivation, rift narrowing, rift geometry, East Shetland Basin

1. Introduction

Continental extension marks the first stage of ocean basin formation, being associated with normal faulting and the development of rift basins (e.g. Nagel and Buck, 2007). Because continental breakup is protracted (i.e. several tens of millions of years; e.g, Ziegler and Cloetingh, 2004), and the related extensional forces are complex, many rifts are products of not one, but multiple phases of extension (e.g., the northern North Sea, Færseth, 1996; the Gulf of Thailand, Morley et al., 2004; and the Galicia rifted margin, Reston, 2005). Unlike polyphase rifts, in which the rheologic character changes due to progressive deformation and thinning during a single extension phase (e.g., fault block rotation and locking, Reston, 2005; ductile to brittle deformation, Lavier and Manatschal, 2006), multiphase rifts have been exposed to multiple episodes of extension (with or without a change in extensional direction), with extension phases possibly separated phases of quiescence.

The geometry and evolution of such multiphase rifts, especially during the latter stages of their development, may thus be controlled by reactivation of discrete, pre-existing, upper crustal structures, such as normal faults, or more pervasive fabrics developed during earlier rift or orogenic periods (e.g., Badley et al., 1988; Strecker et al., 1990; Coward, 1993; Færseth, 1996; Keep and McClay, 1996; Odinsen et al., 2000; Gawthorpe et al., 2003; Morley et al., 2004; Bellahsen and Daniel, 2005; Cowie et al., 2005; Reston, 2005; Henza et al., 2010, 2011; Nixon et al., 2014, Whipp et al., 2014; Duffy et al., 2015; Phillips et al., 2016). However, because sedimentary basins formed during the early stages of multiphase rifting are progressively buried and structurally overprinted during later stages of rifting, it can be difficult to assess the role pre-existing faults play in controlling subsequent rift geometry. In some cases, older faults are abandoned and may in fact be cross-cut by newly formed structures (e.g., Lee and Hwang, 1993; Thomas and Coward, 1995; Reston, 2005; Tomasso et al., 2008; Bell et al., 2014).

Scaled physical models provide useful insights into the geometry and kinematics of upper-crustal, fault networks during multiphase rifts, predicting pre-existing faults are likely to be at least partly reactivated if the stretching direction changes by <45° between extension events (Henza et al., 2010). Although powerful, the majority of these models tend to focus on relatively small fault networks and do not incorporate the superimposed effects of lithosphere-scale heterogeneities (e.g. rheology and temperature). Unlike crustal-scale physical models, lithosphere-scale numerical models can explicitly capture variations in lithosphere properties at a scale appropriate to multiphase rifts associated with continental breakup. Lateral variations in lithosphere rheology and temperature, which may be imposed by and inherited from earlier phases of stretching, may also play a key role in controlling the location and style of rifting (e.g. Buck et al, 1999; Odinsen et al., 2000; Burov and Poliakov, 2001; Huismans et al., 2001; Behn et al., 2002; Ziegler and Cloetingh, 2004; Cowie et al., 2005; Huismans and Beaumont, 2007; Nagel and Buck, 2007; Naliboff and Buiter, 2015). For example, Naliboff and Buiter (2015) use finite difference models to show that, if the period of tectonic quiescence between rift phases is sufficiently long, then the integrated strength of the first-phase rift axis site can recover, leading to large-scale rift migration and the abandonment of first-phase faults. However, most lithosphere-scale models are of insufficient spatial resolution (>1 km) to allow direct investigation of the impact of individual pre-existing faults on the geometry and evolution of subsequent fault networks and the rift basins they control.

Outcrop studies can reveal the geometry and kinematic development of large rift-related fault arrays (i.e., a kinematically linked group of faults that are 10’s to 100 km of length) at a relatively high-level of spatial and temporal precision (e.g., Strecker et al., 1990; Gawthorpe et al., 2003; Morley et al., 2004). However, such studies are typically limited by the quantity and quality of outcrop, with structures and stratigraphy associated with only one rift stage being exposed. In contrast, subsurface studies utilising long (10’s to 100 km), widely spaced (>5 km) 2D seismic profiles allow us to define the basin-scale geometry of structures associated with individual tectonic phases in multiphase rifts, but these lack the spatial detail needed to investigate how pre-existing faults behave on the scale of individual fault systems (i.e., kinematically linked group of faults that are 1-to several 10’s of km long) (e.g., Badley et al., 1988; Coward, 1993; Thomas and Coward, 1995; Færseth, 1996; Reston, 2005). More insightful are subsurface studies using 3D seismic reflection data (e.g., Tomasso et al., 2008; Nixon et al., 2014, Whipp et al., 2014; Duffy et al., 2015). These studies are able to highlight the sometimes subtle influence of pre-existing faults on subsequent fault system development. However, these typically only consider a limited time-interval (<50 Myr) due to the limited depth of imaging, thus do not cover the full multiphase rift history. Furthermore, as individual 3D surveys typically cover only ~500 km^2, these studies are usually too small to assess the relative influence of lithospheric-scale processes.

In this study we combine well log-tied 2D and multiple merged 3D seismic reflection surveys (~10,000 km^2) from the East Shetland Basin, northern North Sea (Fig. 1), to resolve the structure of the basin from pre-Triassic to the present day. Using these observations we address the following questions: (i) do pre-existing normal faults control rift geometry?; and (ii) does the lithosphere thermal and rheological state and structure influence rift geometry?. By addressing these questions, we test the predictions of physical and numerical models of multiphase rifting. Moreover, unlike most previous studies (see above), our extensive, high-quality dataset allows us to document how pre-existing normal faults throughout a regional fault array accommodate later extension.

2. Geological setting

The East Shetland Basin is located in the northern North Sea, on the western flank of the North Viking Graben (Fig. 1a). The present day geometry of the East Shetland Basin is dominated by structures related to the last major phase of rifting during the Middle-to-Late Jurassic. These structures comprise N- to NE-trending, east-dipping normal faults (Cormorant, Pelican, Heather, Murchison, Osprey, Hutton, Ninian, Statfjord, Brent, Strathspey, Alwyn, and Tordis faults) bounding 60–75 km long, 15–25 km wide half-grabens in the middle and eastern part of the East Shetland Basin (Fig. 1c). The East Shetland Platform lies along the western margin of the East Shetland Basin, forming a high that is bounded by two major east-dipping faults (Hudson and West Margin faults), whereas the Tern-Eider Ridge represents a prominent horst block located in the NW of the East Shetland Basin that is flanked by the Tern and Eider faults (Figs. 1c). The Magnus and Tern sub-basins lie to the north and south of the Tern-Eider Ridge, respectively, and the Ninian sub-basin is located in the southern part of the East Shetland Basin (Fig. 1c).

Major phases of basement-involved extension occurred in the Late Palaeozoic to Mesozoic (e.g., Coward, 1990, & 1993, Platt, 1995), with most authors agreeing that the northern North Sea experienced two discrete phases of extension in the Permian-Triassic and Middle-to-Late Jurassic (e.g., Badley et al., 1988; Lee and Hwang, 1993; Thomas and Coward, 1995; Færseth, 1996; Odinsen et al., 2000). The northern North Sea region is a moderately stretched rift, with low β-values i.e. stretching-values). Both extension phases were of approximately the same magnitude, reaching β-values of ~1.4 across the entire width of the northern North Sea, and 1.3 and 1.1 across the East Shetland Basin for the Permian-Triassic and Middle-to-Late Jurassic, respectively (Roberts et al., 1995; Færseth, 1996; Odinsen et al., 2000).

Many authors suggest Late Palaeozoic to Mesozoic rift development was influenced, if not directly controlled, by the inherited Caledonian and Devonian structural framework, both in the East Shetland Basin (Coward, 1990 & 1993; Rattey and Hayward, 1993; Platt, 1995; Thomas and Coward, 1995) and elsewhere (e.g., Doré et al. 1997), although this view has recently been challenged (e.g., Reeve et al., 2013). Reactivation of large Permian-Triassic faults during Middle-to-Late Jurassic rifting throughout the northern North Sea has been proposed (e.g., Badley et al., 1988; Færseth, 1996; Odinsen et al., 2000; Cowie et al. 2005). However, in the East Shetland Basin, an alternative interpretation, envisaging that Permian-Triassic faults are partly cross-cut and only partly reactivated during Middle-to-Late Jurassic rifting, is suggested (e.g., Lee and Hwang, 1993; Thomas and Coward, 1995; Tomasso et al., 2008). For example, Tomasso et al. (2008) propose that west-dipping Triassic normal faults developed in the SE of the East Shetland Basin and were subsequently cross-cut by new, large-displacement, east-dipping faults during Middle-to-Late Jurassic rifting. Tomasso et al. (2008) thus argue that pre-existing Permian-Triassic faults did not control the Middle-to-Late Jurassic rift geometry, at least in this part of the basin.

3. Data and methods

3.1 Seismic Reflection and Well Data

We use a regional compilation of 2D and 3D time-migrated seismic reflection surveys collected between 2006 and 2012 (Fig. 1b). The 2D profiles cover the entire East Shetland Basin, and four partly overlapping, now-merged 3D seismic “merged-surveys” cover almost the whole western margin of the North Viking Graben (Fig. 1b). The 3D seismic reflection merged-surveys image to depths of 4.5 to 6.5 s TWT and have a 12.5 × 12.5 m or 25 × 25 m in-line and cross-line spacing, thus enabling detailed horizon and fault interpretations across much of the East Shetland Basin. The 2D profiles have a line spacing of ~5 km and image to a depth of ~8 s TWT, making them suitable for regional mapping and imaging deeper structures that are not always imaged by the 3D surveys. Data quality ranges from excellent for some of the 3D surveys to moderate for some of the 2D lines. In addition to the seismic reflection data, we use 82 exploration wells (Fig. 1b). These wells contain a standard wireline log suite, including gamma-ray (GR), density (RHOB), sonic (DT), checkshot, chrono- and lithostratrigraphic information, and final well reports. Thirty-nine wells terminate in the Jurassic, 37 in the upper part of the Triassic, and six penetrate the entire Triassic succession (Fig. 1b). The wells have been tied to the seismic data through the construction of synthetic seismograms (Figs. 1b, 2).

3.2 Seismic interpretation

We interpreted nine key horizons across the seismic dataset (6800 km^2) (Figs. 2, 3). With the exception of the pre-Triassic horizons, all horizon interpretations are tied to wells (Figs. 1b, 2). The three pre-Triassic horizons are picked based on their continuous, high-amplitude seismic character; however, because they are not tied to well data, we cannot directly constrain their ages, hence they are named *Pre-Triassic 1*, *2*, and *3*.

To accurately determine the structure and evolution of the East Shetland Basin, structurally complex parts of the basin were interpreted on in-lines and cross-lines spaced at 250 m, and on broadly NE- and NW-trending lines with 625 m spacing. Structurally simpler areas were interpreted on in-lines and cross-lines and/or on broadly NE- and NW-trending lines with 625 m spacing. All faults (n=285) have been interpreted on at least two differently striking seismic lines, one of which trends approximately perpendicular to local fault strike. To improve our interpretation of the major faults (>25 km long) multiple horizontal (time) slices with 300 ms TWT (vertical) spacing were used.

3.3 Time-structure and isochron maps

Time-structure maps of nine key horizons were used to calculate time-thickness (isochron) maps of the eight key stratigraphic intervals. Time-stratigraphic thickness maps are used as a proxy for syn-depositional fault activity because, in rift basins, variations in sediment thickness are predominantly controlled by syn-depositional normal faulting (e.g., McLeod et al., 2000; Childs et al., 2003; Bell et al., 2014). Time-depth data from 79 wells were used to determine an average time-depth relationship; this allowed us to convert thicknesses measured in TWT to metres with an c. 7% error. The principal thickness changes across faults are relatively large (>100 ms TWT across a fault) and therefore the thickness trends are unlikely to change significantly after depth conversion (cf. Tomasso et al., 2008). Furthermore, well data located on the footwall and hanging wall of major faults suggest that no underfilled basins are present in the study area: syn-kinematic sediments were deposited on both the hanging and footwall side of the fault.

4. Sediment thickness distribution and depocentre evolution

We have generated eight isochrons to illustrate temporal and spatial variations in the thickness of key stratigraphic units in the East Shetland Basin (Fig. 4). In addition to structural and stratigraphic geometries observed on the seismic profiles (Figs. 3, 5-8), these isochrons document the pre-Triassic to Cretaceous evolution of the principal rift-related depocentres.

4.1 Unit 1 (Pre-Triassic 1 – Pre-Triassic 2)

Within Unit 1 a number of large (~7 km long by up to 1400 m deep) depocentres are observed in the Magnus, Tern and Ninian sub-basins and in the hanging walls of the NE-trending, Eider and Pelican faults (Fig. 4a, 5). We also observe thinner, but still substantial depocentres (up to 580 m) in the eastern part of the East Shetland Basin, adjacent to the Ninian and Cormorant faults (Figs. 3a, 4a).

4.2 Unit 2 (Pre-Triassic 2 – Pre-Triassic 3)

Depocentres that developed in the Tern sub-basin and hanging wall of the Pelican Fault during the previous time-interval continued to deepen during deposition of Unit 2 (Fig. 4b). The depocentre adjacent to the Ninian Fault, which defined the Ninian sub-basin, became segmented into two (Figs. 3c, 4b, 6a). A large depocentre formed in the hanging wall of the Eider Fault, burying the previously developed Magnus sub-basin (Figs. 3c, 4b). In the hanging wall of the large N- to NE-trending faults located in the middle of the East Shetland Basin (Cormorant, Murchison, Osprey, and Thistle faults), deposits of Unit 2 are relatively thin (~580 m) and fairly isopachous. In the SE of the study area, we observe eastward thickening of this unit towards the crest of the Ninian footwall (Figs. 3b, c, 4b, 6a).

4.3 Teist Formation (Lower Triassic) (ca. 251-245 Ma)

Overall, Lower Triassic deposits are relatively thin in the East Shetland Basin, gradually thickening eastward from ~170 to 520 m, with a few small depocentres in the hanging walls of several of the NE-trending faults (e.g., Pelican, Tern, and Eider faults, and Tern sub-basin; Figs. 3a, 4c). A major depocentre does, however, occur on the western flank of the Ninian sub-basin, with strata thickening westward (up to 1740 m thick) into the immediate hanging wall of the Heather Fault (Figs. 3a, 4c).

4.4 Lomvi and Lunde formations (Middle-to-Upper Triassic) (ca. 245-201 Ma)

There is a clear change in sediment thickness patterns in Middle-to-Upper Triassic deposits described here (Fig. 4d) compared to the older seismic units (Figs. 4a, b, c). For example, in the western part of the basin, rather than being a broadly isopachous depocentre in the hanging wall of the Eider Fault, Middle-to-Upper Triassic deposits define a single, ~840 m thick depocentre towards its southern end, and thinning northward towards the Magnus sub-basin (down to ~500 m) (Figs. 3a, b, 4d, 5). In the footwall of the Eider Fault, Middle-to-Upper Triassic deposits thicken gradually eastward from ~75 m on the Tern-Eider Ridge to ~1200 m south of the Tordis Fault (Figs. 3, 4d, 6, 7).

4.5 Statfjord Formation (uppermost Triassic-to-Lower Jurassic) (ca. 201-192 Ma)

Another major change in sediment thickness distribution occurs during the deposition of the uppermost Triassic-to-Lower Jurassic deposits (Fig. 4e).

Rather than defining a single, large, fault-bound depocentre located on the western margin of the East Shetland Basin, the uppermost Triassic-to-Lower Jurassic sediments vary little in thickness, and are characterized by tabular packages of sub-parallel reflections (Fig. 3, 4e, 8). We note that hanging wall packages are not wedge-shaped; rather, they are tabular like, albeit thicker than, their footwall counterparts resulting in step-wise, across-fault, thickness changes (Fig. 3, 4e, 8). Examples of this style of seismic-stratigraphic geometry occur adjacent to the Cormorant Fault (0 to ~80 m thickness increase), the Ninian, Hutton, Murchison faults (~75 to ~250 m thickness increase), and the Alwyn, Strathspey, Brent, and Statfjord faults ~230 to ~ 475 m thickness increase) (Figs. 3, 4e, 8).

4.6 Dunlin Group (Lower Jurassic) (ca. 192-175 Ma)

The trend of step-wise thickness changes of tabular stratigraphic packages across major N- to NE-trending faults is also observed in Lower Jurassic deposits of the Dunlin Group (Figs. 3, 4f). This is particularly well expressed across the Cormorant Fault (0 to ~85 m thickness increase), Ninian and Hutton faults (0 to ~225 m thickness increase), and Alwyn, Strathspey and Brent faults (~190 to 440 m thickness increase).

4.7 Brent Group (Middle Jurassic) (ca. 175-166 Ma)

During deposition of the overall relatively thin (up to 350 m) Brent Group (Fig. 4g), depocentres not only developed in the hanging walls of most of the N- to

NE-trending, east-dipping faults (Cormorant, Ninian, Hutton, Alwyn, Strathspey, Brent, and Statfjord faults), but also in the hanging walls of the NE-trending Eider, Osprey, Murchison, and Heather faults (Figs. 3, 4g). Thicknesses typically increase from ~75 m on the footwalls of these faults to ~180 – 360 m in the adjacent hanging wall depocentres (Fig. 4g).

4.8 Viking Group (Middle-to-Upper Jurassic) (ca. 166-145 Ma)

At this time, large, 25 km long depocentres (up to 1550 m thick) developed in the hanging walls of the major N- to NE-trending faults across the entire width East Shetland Basin. Prominent wedge-shaped stratigraphic packages define these depocentres (Figs. 3, 4h, 6-8). It should be noted that the Base Cretaceous Unconformity (BCU), which is locally erosional over the footwall crests, defines the top of this stratigraphic package. Calculated thicknesses, thus, represent a minimum value in the footwall crests.

5. Rift-related evolution of the East Shetland Basin

The isochron maps allow us to document the distribution of sediment depocentres through time and space (Fig. 4). In combination with the cross-cutting relationships between faults observed on the seismic data (Figs. 3, 5-8), these isochrons yield a detailed insight on the fault array development throughout the East Shetland Basin (Fig. 9). From the pre-Triassic to Early Triassic, multiple 10 – 20 km long, NNW- to NE-trending, west- and east-dipping faults were active in the middle and western parts of the East Shetland Basin (Figs. 4a-c, 9a-c). These faults formed the boundaries to several large depocentres (~15 by 5 km). The predominant strike of the active faults changed throughout this interval from NNW-SSE and N-S, to NE-SW (Figs. 4a-c, 9a-c), with the latter trend possibly reflecting reactivation of the NE-SW Caledonian structural grain (e.g., Coward, 1990 & 1993; Rattey and Hayward, 1993; Platt, 1995; Thomas and Coward, 1995). We have no direct evidence of the presence of any basement fabrics in our dataset, however.

During the Middle-to-Late Triassic, strain was mainly focused in the west of the East Shetland Basin, being localised on the Eider Fault (Fig. 5, 9d). Elsewhere, syn-depositional faulting ceased, and strata gradually thickened eastward across the East Shetland Basin (Figs. 3, 4d, 6, 7), possibly due to activity on a large west-dipping fault located east of the study area near the axis of the North Viking Graben (e.g., Tomasso et al., 2008). An alternative interpretation is that this gradual eastward thickening of Middle-to-Upper Triassic sediments reflects thermal subsidence associated with Permian-Triassic fault activity in the Horda Platform, which is located on the eastern margin of the North Viking Graben (Fig. 4a) (e.g., Badley et al., 1988; Lee and Hwang, 1993; Thomas and Coward, 1995; Færseth, 1996; Odinsen et al. 2001; Bell et al., 2014).

During the latest Triassic-to-Early Jurassic (Figs. 4e, f, 9e, f), strain mainly focused in the eastern part of the East Shetland Basin on long, N- to NE-trending, east-dipping faults that formed the boundaries to large, ~50 km long and ~25 km wide, half-grabens. Some of these faults represent reactivated pre-Jurassic normal faults (Figs. 4e, f, 6, 9e-g); however, others are new, relatively steep faults, cross-cutting older inactive and buried fault systems (Figs. 4e, f, 6-8, 9e-g). The change from relatively distributed faulting in the centre and western parts of the East Shetland Basin during the pre-Triassic and Triassic, to relatively focused faulting in the eastern part of the basin during the Early-to-Middle Jurassic, documents the onset of the Late Jurassic Viking Graben rift system. Long, N-trending, east-dipping fault systems remain active during the Late Jurassic, and smaller faults mainly develop parallel to the larger faults (Figs. 4b, 7, 9f-h).

Most of the Late Jurassic faults originated no earlier than the latest Triassic, or were newly formed in the Late Jurassic (Fig. 4e, 9e). The main pre-Jurassic faults either: (i) became inactive, were buried, and, in some cases, were cross-cut by faults developed during the Jurassic (e.g., Ninian and Tern sub-basins, Figs. 3b, c, 6, 9); or (ii) underwent only minor reactivation relative to the newly formed major faults during the main period of Late Jurassic rifting (e.g., Magnus sub-basin, Figs. 4a, h, 7, 8).

6 Discussion

6.1 Do pre-existing normal faults control rift geometry?

Physical models, and several field and subsurface-based studies, suggest that structures produced by an earlier phase of extension strongly control the pattern of faulting and rift geometry. In areas where dip angle, dip direction and stress conditions are favourable, earlier developed faults will be prone to reactivation (e.g., Keep and McClay, 1996; Morley et al., 2004; Bellahsen and

Daniel, 2005; Henza et al., 2010 & 2011; Whipp et al., 2014; Duffy et al., 2015). However, this relationship can be complex; for example, some or only parts of the earlier developed fault array may be reactivated (Lee and Hwang, 1993; Thomas and Coward, 1995; Tomasso et al., 2008), and/or fault reactivation may be strongly diachronous (e.g., Bell et al., 2014). Our study shows that many earlier developed faults in the East Shetland Basin were not reactivated, but cross-cut by newly formed, relatively steep-dipping faults, during subsequent extension (Figs. 4e, f, 5, 6-8), and thus played only a minor role in controlling the subsequent rift geometry. This directly challenges the view forwarded by most previous studies that do suggest key control of earlier developed faults on subsequent rift geometry (e.g., Badley et al., 1988; Coward 1990 & 1993; Lee and Hwang, 1993; Rattey and Hayward, 1993; Færseth, 1996; Odinsen et al., 2000; Cowie et al., 2005; Henza et al., 2010 & 2011; Nixon et al. 2014; Whipp et al., 2014; Duffy et al., 2015). Rock mechanics suggests that, once formed, faults typically represent a plane of weakness (Sibson, 1985), with less stress being required to reactivate them than to create new faults (e.g., Ranalli and Yin, 1990; Yin and Ranalli, 1992; Faccenna et al., 1995). In the East Shetland Basin we note that limited reactivation of pre-existing faults may reflect fault strengthening due to fluid-rock reactions and fault zone diagenesis (e.g., Tenthorey and Cox, 2006; Naliboff and Buiter, 2015) and/or a lower angle fault dip due to rotation of several earlier developed faults as the result of burial, making the pre-existing faults less favourable for reactivation (e.g., Ranalli and Yin, 1990; Yin and Ranalli, 1992; Morley, 1999). The results of our study are thus broadly consistent with those of Tomasso et al. (2008), who argue that fault activity during a first rift phase (Triassic) was mostly focused on N-trending, west-dipping faults, which subsequently were cross-cut by N-trending, east-dipping faults during the a second rift phase (Middle-to-Late Jurassic). However, in terms of timing, we found no convincing evidence for Triassic age, N-trending, west-dipping faults in the SE of the East Shetland Basin. Using our regional dataset, we demonstrate that Triassic rifting did not occur in the east of the East Shetland Basin. Our observations suggest Triassic development of a single large N-trending, west dipping fault on the western margin of the East Shetland Basin. In the footwall of this large fault Triassic deposits gradually thicken eastward, reflecting rift activity east of the East Shetland Basin, in the North Viking Graben or on the Horda Platform (Figs. 3, 4d, 5-8).

Nevertheless, in the context of the influence of pre-existing normal faults, the mechanical characteristics as a result of subsequent burial, compaction, and associated rotation to lower dips are thus important, as these may make a fault less favourable for reactivation. The impact of these mechanical characteristics during rifting, however, are not typically directly incorporated in physical models of multiphase rifting (e.g., Keep and McClay, 1996; Bellahsen and Daniel, 2005; Henza et al., 2010, 2011; Agostini et al., 2011). This modelling limitation is important, because it suggests such models potentially overestimate the importance of fault reactivation during multiphase rifting.

6.2 Does the lithosphere thermal and rheological state and structure influence rift geometry?

The recognition that reactivation of earlier developed faults was limited throughout the East Shetland Basin, indicates that the presence of pre-existing faults is not always a major control on rift geometry development. Heterogeneity in the mechanical characteristics of earlier developed faults (see section 6.1), and moreover, the observed migration of strain throughout the development of the East Shetland Basin (see section 5) suggests that rift geometry is likely affected by processes other than crustal-scale heterogeneity. Lithosphere-scale numerical models suggest that the thermal evolution and structure of the asthenosphere and subcrustal lithosphere affects rift-related crustal deformation (e.g., Buck et al, 1999; Odinsen et al., 2000; Huismans et al., 2001; Behn et al., 2002; Cowie et al., 2005; Nagel and Buck, 2007). For example, using a finite element model Behn et al. (2002) predict that, when no regional temperature gradient is imposed on the part of the crust being stretched, deformation will be distributed between several conjugate fault systems forming a relatively wide rift. In contrast, in the presence of a horizontally varying temperature field, perhaps imposed by an earlier rift event, rift-related faulting focuses where the lithosphere is thinnest (Behn et al., 2002). Cowie et al. (2005) expand on this numerical model and link this prediction to the eastern part of the East Shetland Basin. They demonstrate a gradual change from distributed faulting to localised faulting on large, N-trending, east-dipping faults, and finally to large-scale strain migration into the Viking Graben during Middle-Late Jurassic rifting (Fig. 1a). Based on numerical modelling, Cowie et al. (2005) suggest that the strain migration is a result of horizontal variations in the lithospheric temperature field. We observe a broadly similar style of large-scale strain migration throughout the entire

East Shetland Basin (Fig. 10). However, Cowie et al. (2005) suggest that the strain migration occurs during the Middle Jurassic-to-earliest Cretaceous reactivating Permian-Triassic faults, while we show that, rather than two discrete phases of extension separated by a period of tectonic quiescence, the East Shetland Basin developed in response to a single, somewhat protracted phase of rifting (~150 Myr) from pre-Triassic to Cretaceous with limited reactivation (Fig. 10). Nevertheless we draw a similar conclusion to Cowie et al., (2005), that the Middle-to-Late Jurassic geometry of the northern North Sea is strongly influenced by the evolving thermal structure of the lithosphere, leading to strain localization in the upper crust.

Although our study and that of Cowie et al. (2005) are limited to the western margin of the northern North Sea rift, our results support predictions of the tectonostratigraphic forward model of Odinsen et al. (2000). They suggest the thermal structure of the lithosphere across the whole northern North Sea rift reflects differences between the Permian-Triassic and Jurassic extension: a wide thermal perturbation during the Permian-Triassic, and a narrow thermal perturbation, focused under the North Viking Graben, during the Jurassic (Fig. 10). Moreover, our results are consistent with those of Bell et al. (2014), who show that faulting patterns on the Norwegian margin of the North Viking Graben are not solely controlled by reactivation of underlying, Permian-Triassic faults. Bell et al. (2014), also speculate that the larger rift geometry was primarily affected by the thermal and rheological evolution of the lithosphere and variations in the regional stress field.

Rifting is typically described using two end-members, where *passive* rifting is driven by far-field extensional stresses and the space created by lithosphere thinning is passively filled by the atmosphere, and *active* rifting is driven by active mantle plume impingement on the base of the lithosphere (e.g., Huismans et al. 2001). However, multiple studies based on 2D plain-strain thermo-mechanical finite-element models, describe *rift narrowing* during symmetrical continental rifting, whereby a change from wide, passive extension to narrow, active extension might take place during the late syn-rift and or post-rift (e.g., Huismans et al., 2001; Huismans and Beaumont 2007; Nagel and Buck, 2007). Rift narrowing, thus, involves an evolving thermal and rheological lithosphere during rifting. We therefore argue that the pre-Triassic to Cretaceous eastward strain migration we document in the East Shetland Basin demonstrates a natural example of rift narrowing. Even though the time interval of the numerical models (e.g., 40 Myr full rift, Huismans et al., 2001) is smaller than the northern North Sea rift phase (~150 Myr failed rift, Færseth, 1996), the results of Huismans et al. (2001), Huismans and Beaumont (2007), and Nagel and Buck (2007), arguably demonstrate a progressive change from a wide to narrower rift, as observed by previous studies (e.g., Færseth, 1996; Odinsen et al., 2000; Cowie et al., 2005; Bell et al., 2014) and our study (Figs. 4, 10). We draw on the predictions of the previous numerical models to suggest that in the northern North Sea the observed gradual change in rift style from wide to narrow is more likely to be the result of the lithospheric thermal and rheological evolution prior to the Late Jurassic rift maximum phase, rather than the interaction of pre-Jurassic and Jurassic rift structures as suggested by previous work (e.g., Badley et al., 1988; Coward, 1993; Færseth, 1996). We interpret that narrowing of the rift is associated with the evolving thermal and rheological structure of the lithosphere. Although pre-existing structures are able to influence subsequent rift-related structures, the larger lithosphere-scale thermal and rheologic heterogeneity may serve to dilute their control on rift geometry.

7. Conclusion

Our observations in the East Shetland Basin, northern North Sea, demonstrate that pre-existing rift related faults may have a much more limited control on rift geometry and evolution in multiphase rifts than previously believed. Using a regional, high quality, subsurface dataset, we document how only few pre-existing faults reactivate, while most are buried and/or cross-cut by younger rift-related faults during a protracted, pre-Triassic to Cretaceous rift phase. We argue that limited reactivation may reflect fault strengthening and/or fault dip rotation due to the burial and compaction. Moreover, we suggest that the upper crustal strain migration and rift narrowing is a result of the evolving lithosphere, which is in accordance with predictions of lithosphere-scale numerical models of continental break-up and rifting. Although the control of pre-existing faults is clearly observed in natural examples on the scale of a fault system (e.g., Whipp et al., 2014; Duffy et al., 2015), we propose that on a rift scale this influence might be overestimated and less important than lithosphere-scale variations thermal and rheological characteristics as predicted by lithosphere-scale numerical models (e.g., Huismans et al., 2001; Huismans and Beaumont 2007; Nagel and Buck, 2007). We, therefore, caution against the application of predictions from analogue models, which do not include the role of lithospheric thermal and rheological evolution.

Acknowledgements

This work is funded by a Statoil Departmental Scholarship at Imperial College London and the MultiRift Project, which is funded by the Research Council of Norway (PETROMAKS Project number 215591/E30) and Statoil to the University of Bergen, and partners Imperial College London, University of Manchester and University of Oslo. We thank editor Rebecca Bendick, and two anonymous reviewers for their constructive reviews Al Fraser and Jon Bull are thanked for their comments on earlier versions of this manuscript. For their involvement in providing the subsurface data and the permission to publish, we are grateful to Thomas Weight, Tom Dreyer, Mark Lawson, Claire Thomas, and Bart Hendriks at Statoil, Richard Lamb at PGS, and Bent Kjølhamar at TGS. Schlumberger is thanked for providing Petrel to Imperial College. We thank the members of the Basins Research Group at Imperial College London and the MultiRift Project, especially Thilo Wrona, for useful discussion.

References

Agostini, A., Bonini, M., Corti, G., Sani, F., & Mazzarini, F., 2011, *Fault architecture in the Main Ethiopian Rift and comparison with experimental models: Implications for rift evolution and Nubia–Somalia kinematics*, Earth and Planetary Science Letters, 301, 479-492. http://dx.doi.org/10.1016/j.epsl.2010.11.024

Badley, M. E., Price, J. D., Rambech Dahl, C., and Agdestein, T., 1988, *The structural evolution of the northern Viking Graben and its bearing upon extensional modes of basin formation*, J. Geol. Soc., 145, 455-472. http://dx.doi.org/10.1144/gsjgs.145.3.0455

Behn, M. D., Lin, J. and Zuber, M. T., 2002, *A continuum mechanics model for normal faulting using a strain-rate softening rheology: implications for thermal and rheological controls on continental and oceanic rifting*, Earth and Planetary Science Letters, 202, 725-740. http://dx.doi.org/10.1016/S0012-821X(02)00792-6

Bell, R. E., Jackson, C. A-L., Whipp, P. S., and Clements, B., 2014, *Strain migration during multiphase extension: Observations from the northern North Sea*, Tectonics, 33, 1936-1963. http://dx.doi.org/10.1002/2014TC003551

Bellahsen, N., and Daniel, J. M., 2005, *Fault reactivation control on normal fault growth: an experimental study*, Journal of Structural Geology, 27, 769-780. http://dx.doi.org/10.1016/j.jsg.2004.12.003

Buck, W. R., Lavier, L. L., and Poliakov, A. N. B., 1999, *How to make a rift wide,* Philosophical Transactions of the Royal Society of London, Series A: Mathematical, Physical and Engineering Sciences, 357, 671-693. https://doi.org/10.1098/rsta.1999.0348

Childs, C., A. Nicol, J. J. Walsh, and J. Watterson, 2003, *The growth and propagation of synsedimentary faults*, J. Struct. Geol., 25, 633-648. http://dx.doi.org/10.1016/S0191-8141(02)00054-8

Coward, M. P., 1990, *The Precambrian, Caledonian and Variscan framework to NW Europe*, Geological Society, London, Special Publications, 55, 1-34. http://dx.doi.org/10.1144/GSL.SP.1990.055.01.01

Coward, M. P., 1993, *The effect of Late Caledonian and Variscan continental escape tectonics on basement structure, Paleozoic basin kinematics and subsequent Mesozoic basin development in NW Europe.* In: Geological Society, London, Petroleum Geology Conference series, Geological Society of London, 1095-1108. http://dx.doi.org/10.1144/0041095

Cowie, P. A., Underhill, J. R., Behn, M. D., Lin, J., and Gill, C. E., 2005, *Spatio-temporal evolution of strain accumulation derived from multi-scale observations of Late Jurassic rifting in the northern North Sea: A critical test of models for lithospheric extension*, Earth and Planetary Science Letters, 234, 401-419. http://dx.doi.org/10.1016/j.epsl.2005.01.039

Doré, A.G., Lundin, E.R., Fichler, C. and Olesen, O., 1997, *Patterns of basement structure and reactivation along the NE Atlantic margin,* Journal of the Geological Society, 154, pp.85-92. http://dx.doi.org/10.1144/gsjgs.154.1.0085

Duffy, O.B., Bell, R.E., Jackson, C.A., Gawthorpe, R.L. and Whipp, P.S., 2015, *Fault growth and interactions in a multiphase rift fault network:*

Horda Platform, Norwegian North Sea, Journal of Structural Geology, 80, pp.99-119. http://dx.doi.org/10.1016/j.jsg.2015.08.015

Faccenna, C., Nalpas, T., Brun, J.P., Davy, P. and Bosi, V., 1995, *The influence of pre-existing thrust faults on normal fault geometry in nature and in experiments.* Journal of Structural Geology, 17, pp.1139-1149. http://dx.doi.org/10.1016/0191-8141(95)00008-2

Færseth, R. B., 1996, *Interaction of Permo-Triassic and Jurassic extensional fault-blocks during the development of the northern North Sea*, Journal of the Geological Society, 153, 931-944. http://dx.doi.org/10.1144/gsjgs.153.6.0931

Gawthorpe, R.L., Jackson, C.A.L., Young, M.J., Sharp, I.R., Moustafa, A.R. and Leppard, C.W., 2003, *Normal fault growth, displacement localisation and the evolution of normal fault populations: the Hammam Faraun fault block, Suez rift, Egypt,* Journal of Structural Geology, 25, pp.883-895. http://dx.doi.org/10.1016/S0191-8141(03)00059-2

Henza, A. A., Withjack, M. O., and Schlische, R. W., 2010, *Normal-fault development during two phases of non-coaxial extension: An experimental study*, Journal of Structural Geology, 32, 1656-1667. http://dx.doi.org/10.1016/j.jsg.2009.07.007

Henza, A. A., Withjack, M. O., and Schlische, R. W., 2011, *How do the properties of a pre-existing normal-fault population influence fault development during a subsequent phase of extension?*, Journal of Structural Geology, 33, 1312-1324. http://dx.doi.org/10.1016/j.jsg.2011.06.010

Huismans, R. S., Podladchikov, Y. Y. and Cloetingh, S. A. P. L., 2001, *The transition from passive to active rifting, relative importance of asthenospheric doming and passive extension of the lithosphere*, Journal of Geophysical Research, 106, 11,271-11,291. http://dx.doi.org/10.1029/2000JB900424

Huismans, R. S., Beaumont, C. 2007, *Roles of lithospheric strain softening and heterogeneity in determining the geometry of rifts and continental margins*, Geol. Soc. London Spec. Publ., 282, 111-138. http://dx.doi.org/10.1144/SP282.6

Keep, M., and McClay, K.R., 1997, *Analogue modelling of multiphase rift systems*, Tectonophysics, 273, 239-270. http://dx.doi.org/10.1016/S0040-1951(96)00272-7

Lavier, L. L., & Manatschal, G., 2006, *A mechanism to thin the continental lithosphere at magma-poor margins*, Nature, 440(7082), 324-328. http://dx.doi.org/10.1038/nature04608

Lee, M. J., and Hwang, Y. J., 1993, *Tectonic evolution and structural styles of the East Shetland Basin.* Geological Society of London, Petroleum Geology Conference series, 4, 1137-1149. http://dx.doi.org/10.1144/0041137

McLeod, A. E., Dawers, N. H., and Underhill, J. R., 2000, *The propagation and linkage of normal faults: Insights from the Strathspey–Brent–Statfjord fault array, northern North Sea*, Basin Research, 12, 263-284. http://dx.doi.org/10.1111/j.1365-2117.2000.00124.x

Morley, C.K., 1999. How successful are analogue models in addressing the influence of pre-existing fabrics on rift structure?, *Journal of Structural Geology*, *21*, pp.1267-1274. http://dx.doi.org/10.1016/S0191-8141(99)00075-9

Morley, C. K., Haranya, C., Phoosongsee, W., Pongwapee, S., Kornsawan, A., and Wonganan, N., 2004, *Activation of rift oblique and rift parallel pre-existing fabrics during extension and their effect on deformation style: examples from the rifts of Thailand*, Journal of Structural Geology, 26, 1803-1829. http://dx.doi.org/10.1016/j.jsg.2004.02.014

Nagel, T.J., and Buck, W.R., 2007, *Control of rheological stratification on rifting geometry: a symmetric model resolving the upper plate paradox*, International Journal of Earth Science, 96, 1047-1057. http://dx.doi.org/10.1007/s00531-007-0195-x

Naliboff, J., and Buiter, S.J.H., 2015, *Rift reactivation and migration during multiphase extension*, Earth and Planetary Science Letters, 421, 58-67. http://dx.doi.org/10.1016/j.epsl.2015.03.050

Nixon, C. W., Bull, J. M., & Sanderson, D. J., 2014, *Localized vs distributed deformation associated with the linkage history of an active normal fault, Whakatane Graben, New Zealand*, Journal of Structural Geology, 69, 266-280. http://dx.doi.org/10.1016/j.jsg.2014.06.005

Odinsen, T., Reemst, P., Van der Beek, P., Faleide, J. I., and Gabrielsen, R. H., 2000, *Permo-Triassic and Jurassic extension in the northern North Sea: results from tectonostratigraphic forward modelling, Dynamics of the Norwegian Margin*, Geological Society, London, Special Publications 167, 83-103. http://dx.doi.org/10.1144/GSL.SP.2000.167.01.05

Phillips, T.B., Jackson, C.A., Bell, R.E., Duffy, O.B. and Fossen, H., 2016, *Reactivation of intrabasement structures during rifting: A case study from offshore southern Norway,* Journal of Structural Geology, 91, pp. 54-73. http://dx.doi.org/10.1016/j.jsg.2016.08.008

Platt, N. H. 1995, *Structure and tectonics of the northern North Sea: new insights from deep penetration regional seismic data,* Geological Society, London, Special Publications, 80, 103-113. http://dx.doi.org/10.1144/GSL.SP.1995.080.01.05

Ranalli, G., Yin, Z.M., 1990, *Critical stress difference and orientation of faults in rocks with strength anisotropies: the two-dimensional case*, Journal of Structural Geology 12, 1067-1071. http://dx.doi.org/10.1016/0191-8141(90)90102-5

Rattey, R. P., and Hayward, A. B., 1993, *Sequence stratigraphy of a failed rift system: the Middle Jurassic reservoir distribution within the UK central North Sea*, In: R. J. Parker (Ed.), Petroleum geology of northwest Europe: London, Geological Society, 215-250. http://dx.doi.org/10.1144/0040215

Reeve, M. T., Bell, R. E., and Jackson, C. A-L., 2013, *Origin and significance of intra-basement reflections offshore western Norway*, J. Geol. Soc., 171, 1-4. http://dx.doi.org/10.1144/jgs2013-020

Reston, T. J., 2005, *Polyphase faulting during the development of the west Galicia rifted margin*, Earth and Planetary Science Letters, 237, 561-576. http://dx.doi.org/10.1016/j.epsl.2005.06.019

Roberts, A. M., Yielding, G., Kusznir, N. J., Walker, I. M., & Dorn-Lopez, D., 1995, *Quantitative analysis of Triassic extension in the northern Viking Graben,* Journal of the Geological Society, 152, 15-26. http://dx.doi.org/10.1144/gsjgs.152.1.0015

Sibson, R.H., 1985, *A note on fault reactivation,* Journal of Structural Geology, 7, pp.751-754. http://dx.doi.org/10.1016/0191-8141(85)90150-6

Strecker, M. R., Blisniuk, P. M., and Eisbacher, G. H., 1990, *Rotation of extension direction in the central Kenya Rift*, Geology, 18, 299-302. http://dx.doi.org/10.1130/0091-7613(1990)018<0299:ROEDIT>2.3.CO;2

Tenthorey, E. and Cox, S.F., 2006, *Cohesive strengthening of fault zones during the interseismic period: An experimental study,* Journal of Geophysical Research: Solid Earth, 111(B9). http://dx.doi.org/10.1029/2005JB004122

Thomas, D. W., and Coward, M.P, 1995, *Late Jurassic-Early Cretaceous inversion of the northern East Shetland Basin, northern North Sea*, Geological Society, London, Special Publications, 88, 275-306. http://dx.doi.org/10.1144/GSL.SP.1995.088.01.16

Tomasso, M., Underhill, J. R., Hodgkinson, R. A., and Young, M. J., 2008, *Structural styles and depositional architecture in the Triassic of the Ninian and Alwyn North fields: Implications for basin development and prospectivity in the Northern North Sea*, Marine and Petroleum Geology, 25, 7, 588-605. http://dx.doi.org/10.1016/j.marpetgeo.2007.11.007

Whipp, P. S., Jackson, C., Gawthorpe, R. L., Dreyer, T., and Quinn, D., 2014, *Normal fault array evolution above a reactivated rift fabric; a subsurface example from the northern Horda Platform, Norwegian North Sea*, Basin Research, 26, 523-549. http://dx.doi.org/10.1111/bre.12050

Yin, Z.M., Ranalli, G., 1992, *Critical stress difference, fault orientation and slip direction in anisotropic rocks under non-Andersonian stress systems,* Journal of Structural Geology 14, 237-244. http://dx.doi.org/10.1016/0191-8141(92)90060-A

Ziegler, P. A., and Cloetingh, S., 2004, *Dynamic processes controlling evolution of rifted basins*, Earth Sci. Rev., 64, 1-50. http://dx.doi.org/10.1016/S0012-8252(03)00041-2

Figure captions

Figure 1: a) Major tectonic elements of the northern North Sea (after Færseth, 1996; Bell et al., 2014). b) Outlines of dataset used for this study. All wells are tied to the seismic data and contain stratigraphic data for the Jurassic (blue), Jurassic and Top Triassic (purple), and Jurassic and Triassic (red). c) Time-structure map of the Top Lunde Formation with major structural elements and faults: Alw = Alwyn Fault, Bre = Brent Fault, Cor = Cormorant Fault, Eid = Eider Fault, ESP = East Shetland Platform, Hea = Heather Fault, Hud = Hudson Fault, Hut = Hutton Fault, MSB = Magnus sub-basin, Mur = Murchison Fault, Nin = Ninian, NSB = Ninian sub-basin, Osp = Osprey Fault, Pel = Pelican Fault, Sta = Statfjord Fault, Str = Strathspey, TER = Tern-Eider Ridge, Ter = Tern Fault, TSB = Tern sub-basin, Thi = Thistle Fault, Tor = Tordis Fault, W-M = West Margin Fault. The faults and structural features are named after the adjacent hydro-carbon bearing fields.

Figure 2: Stratigraphic column of the East Shetland Basin (modified after Fæseth, 1996). Showing the interpreted horizons and synthetic well ties Proposed sequence stratigraphy is based on Rattey and Hayward (1993). See Figure 5.1 for well locations. Depth = TVD, GR = Gamma Ray, RHOB = Density, DT = Sonic, RC = Reflection Coefficient, AI = Acoustic Impedance.

Figure 3: Three interpreted 2D Time-migrated seismic reflection profiles crossing the study area in the a) north, b) centre, and c) south. The seismic profiles including well penetrations and major faults and structural features. See Figures 1b for locations.

Figure 4: Isochrons overlain by fault polygons that offset the top surface (left) with line drawing of faults over outline of 3D seismic data coverage (grey polygons) (right) of a) Unit 1, b) Unit 2, c) Teist Formation, d) Lomvi and Lunde formations, e) Statford Formation, f) Dunlin Group, g) Brent Group h) Viking Group. Colours are based on the maximum and minimum thickness value in ms TWT per isochron. Contour interval on all the isochrons is 100 ms TWT. Hatched areas show locations where the top horizon is eroded. See caption of Figure 1 for abbreviated fault and structural features names. See Figure 1c for location.

Figure 5: Seismic section crossing the west-dipping Eider Fault, showing periods of fault growth. For location see Figure 1c, and for horizon abbreviations see Figure 3.

Figure 6: a) Seismic section crossing the Ninian sub-basin and the reactivated Ninian Fault showing an example of the burial of older structures.

b) Seismic section crossing the Ninian sub-basin and reactivated Ninian Fault showing an older fault cross-cut by a younger fault. Growth periods are marked by white lines, and the eastward Triassic thickening direction is marked by the white dashed arrows. For location see Figure 1c, and for horizon abbreviations see Figure 3.

Figure 7: Seismic section crossing the Cormorant and Hutton faults showing an older fault cross-cut by a younger fault and burial of older structures. Growth periods are marked by white lines, and the eastward Triassic thickening direction is marked by the white dashed arrows. For location see Figure 1c, and for horizon abbreviations see Figure 3.

Figure 8: Seismic section crossing the Osprey and Hutton faults showing an older fault cross-cut by a younger fault. Growth periods are marked by white lines. For location see Figure 1c, and for horizon abbreviations see Figure 3.

Figure 9: Schematic block diagrams showing the evolution of the East Shetland Basin. From Pre-Triassic to Middle Triassic, strain is distributed across the whole basin (a-c). During the Middle-to-Late Triassic, strain is focussed on the western part of the basin (d). Strain switches to the eastern part of the basin during Latest Triassic-to-Middle Jurassic (e). Strain remains focussed on the eastern part of the basin throughout the Jurassic (f-h) Faults are coloured according to subsequent development of the basin.

Figure 10: Diagram showing the crustal evolution of the East Shetland Basin (colour) and the proposed evolution of the underlying lithosphere across the northern North Sea (grey scale) showing the transition from wide to narrow rifting (modified after Nagel and Buck, 1997). Strain migration through the East Shetland Basin is marked by the grey scale above the coloured zoom-ins per stage: darker grey indicates the location of relative high strain. a) Wide rift with strain distributed across the whole northern North Sea leading to faulting throughout the entire East Shetland Basin. b) Wide rift with possible focus below the Horda Platform. In the East Shetland Basin, strain is concentrated in the western part, reactivating the Eider Fault, while deposits in its footwall are thickening towards the east. c) Rifting is narrowing with its rift axis below the Viking Graben east of the East Shetland Basin. Strain switches to the eastern part of the East Shetland Basin where new faults initiate and some older faults reactivate near the rift axis. d) Rift maximum stage during narrow rifting with rift axis below the Viking Graben. In the East Shetland Basin, strain is increasing towards the eastern part, faults are reactivating, while new fault are initiating, sometimes burying or cross-cutting older pre-existing normal faults.

Figure 1

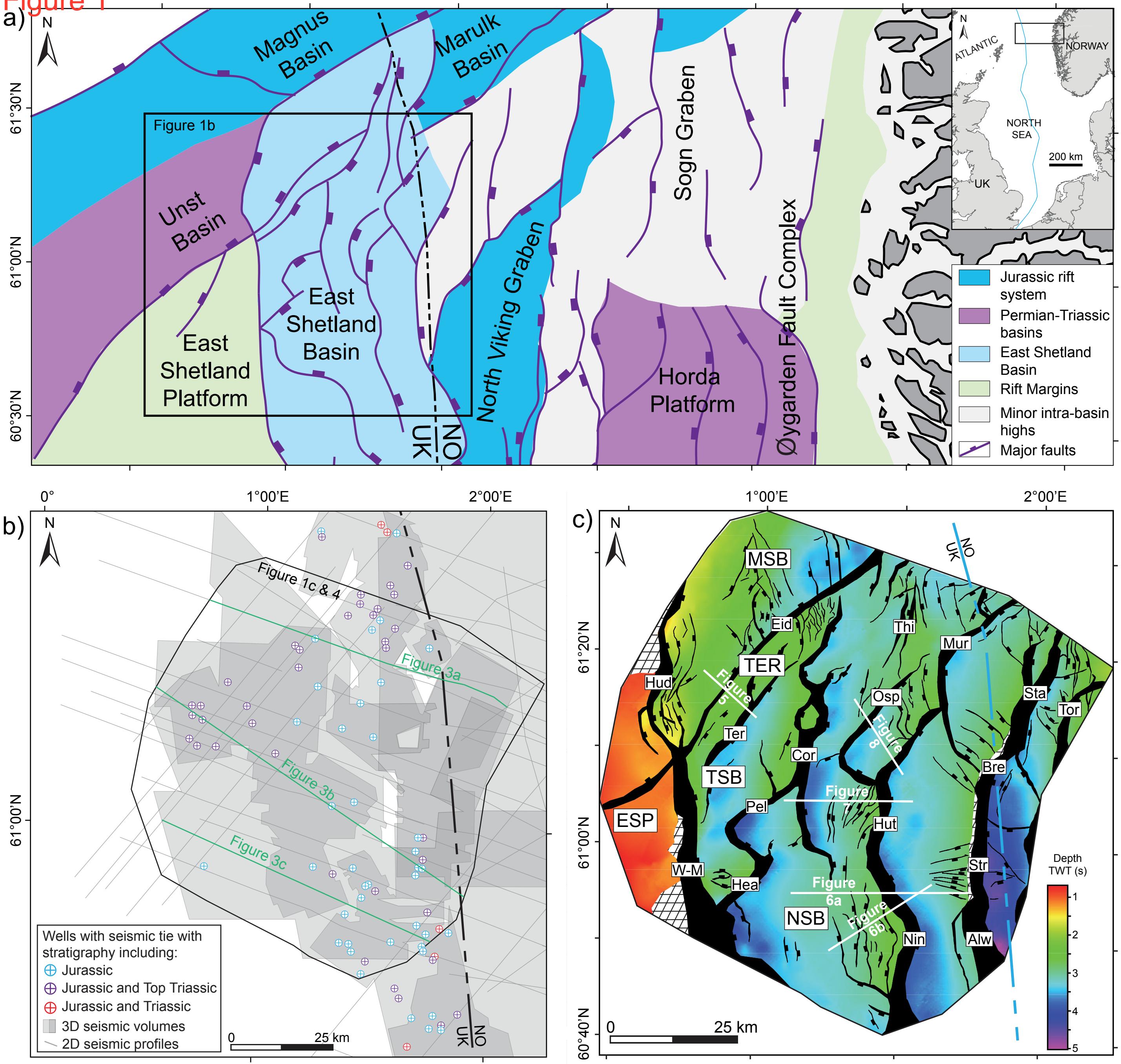
a)
Magnus Basin
Marulk Basin
Sogn Graben
Unst Basin
East Shetland Basin
East Shetland Platform
North Viking Graben
Horda Platform
Øygarden Fault Complex
Figure 1b
NO
UK
ATLANTIC
NORWAY
NORTH SEA
UK
200 km
Jurassic rift system
Permian-Triassic basins
East Shetland Basin
Rift Margins
Minor intra-basin highs
Major faults
0°
2°00'E
4°00'E
6°00'E
61°30'N
61°00'N
60°30'N
b)
Figure 1c & 4
Figure 3a
Figure 3b
Figure 3c
Wells with seismic tie with stratigraphy including:
Jurassic
Jurassic and Top Triassic
Jurassic and Triassic
3D seismic volumes
2D seismic profiles
0
25 km
1°00'E
c)
MSB
TER
TSB
ESP
NSB
Eid
Thi
Mur
Hud
Osp
Sta
Tor
Ter
Cor
Bre
Pel
Hut
W-M
Hea
Str
Nin
Alw
Figure 5
Figure 8
Figure 7
Figure 6a
Figure 6b
Depth TWT (s)
61°20'N
60°40'N

Figure 2

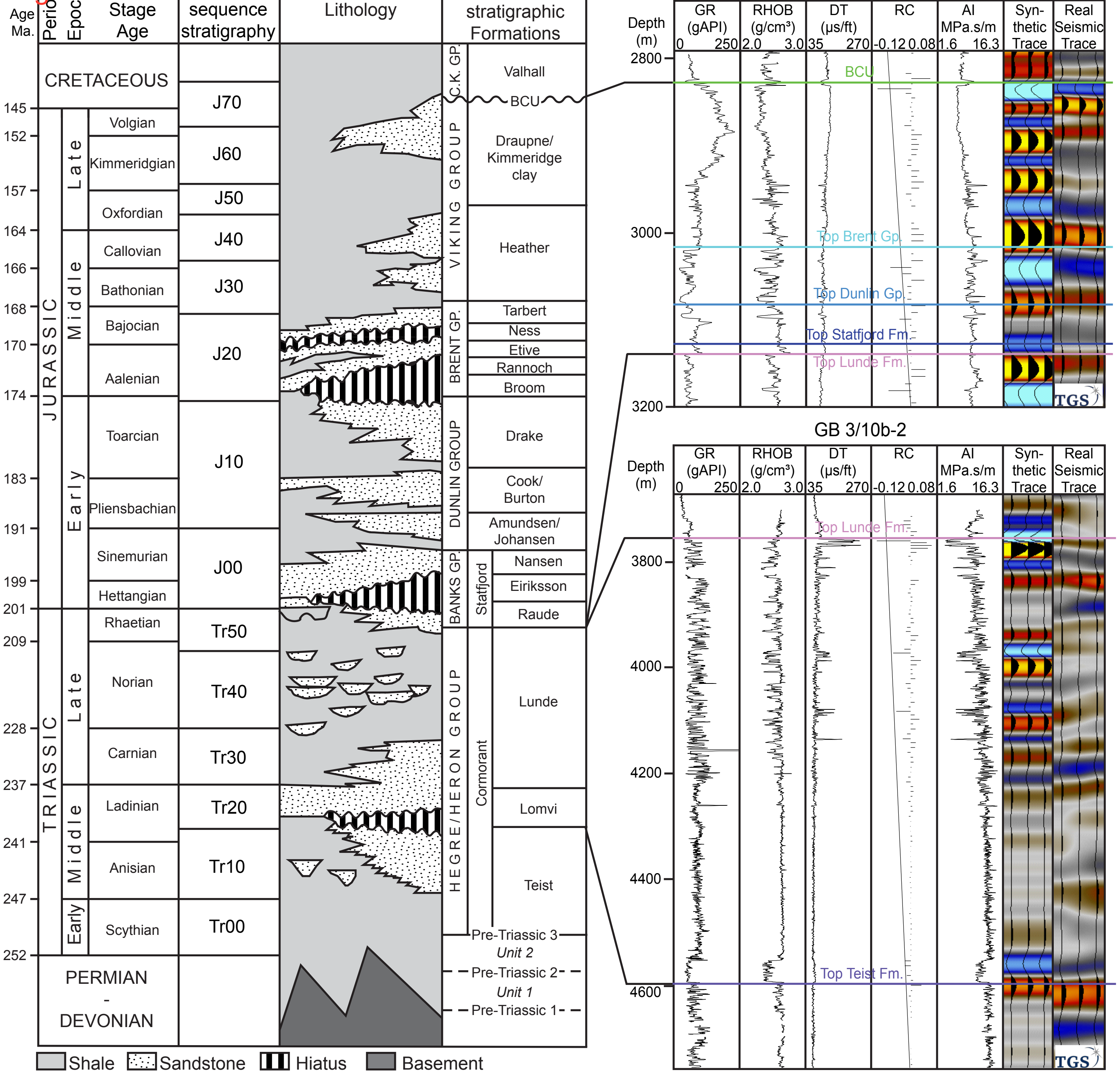

Age Ma.
Period
Epoch
Stage Age
Proposed sequence stratigraphy
Lithology
Litho-stratigraphic Formations
CRETACEOUS
145
152
157
164
166
168
170
174
183
191
199
201
209
228
237
241
247
252
JURASSIC
TRIASSIC
Late
Middle
Early
Volgian
Kimmeridgian
Oxfordian
Callovian
Bathonian
Bajocian
Aalenian
Toarcian
Pliensbachian
Sinemurian
Hettangian
Rhaetian
Norian
Carnian
Ladinian
Anisian
Scythian
PERMIAN - DEVONIAN
J70
J60
J50
J40
J30
J20
J10
J00
Tr50
Tr40
Tr30
Tr20
Tr10
Tr00
C.K. GP.
VIKING GROUP
BRENT GP.
DUNLIN GROUP
BANKS GP.
Statfjord
HEGRE/HERON GROUP
Cormorant
Valhall
BCU
Draupne/ Kimmeridge clay
Heather
Tarbert
Ness
Etive
Rannoch
Broom
Drake
Cook/ Burton
Amundsen/ Johansen
Nansen
Eiriksson
Raude
Lunde
Lomvi
Teist
Pre-Triassic 3
Unit 2
Pre-Triassic 2
Unit 1
Pre-Triassic 1
Shale
Sandstone
Hiatus
Basement
GB 211/26-5A
Depth (m)
GR (gAPI) 0 250
RHOB (g/cm³) 2.0 3.0
DT (µs/ft) 35 270
RC -0.12 0.08
AI MPa.s/m 1.6 16.3
Syn-thetic Trace
Real Seismic Trace
2800
3000
3200
BCU
Top Brent Gp.
Top Dunlin Gp.
Top Statfjord Fm.
Top Lunde Fm.
TGS
GB 3/10b-2
Depth (m)
GR (gAPI) 0 250
RHOB (g/cm³) 2.0 3.0
DT (µs/ft) 35 270
RC -0.12 0.08
AI MPa.s/m 1.6 16.3
Syn-thetic Trace
Real Seismic Trace
3800
4000
4200
4400
4600
Top Lunde Fm.
Top Teist Fm.
TGS

Figure 3

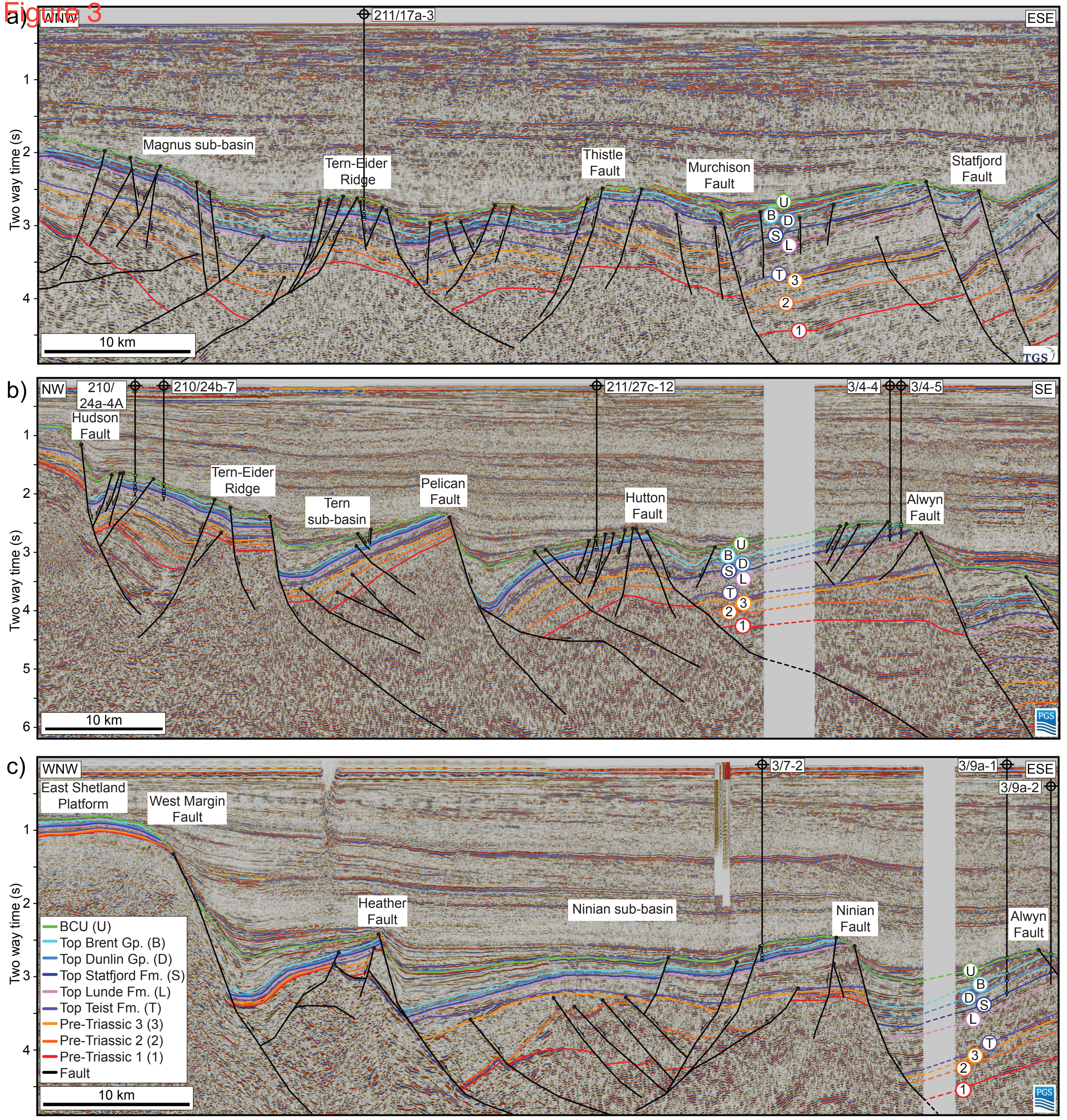

a)
WNW
211/17a-3
ESE
Two way time (s)
Magnus sub-basin
Tern-Eider Ridge
Thistle Fault
Murchison Fault
Statfjord Fault
U
B
D
S
L
T
3
2
1
10 km
TGS
b)
NW
210/24a-4A
210/24b-7
211/27c-12
3/4-4
3/4-5
SE
Hudson Fault
Tern-Eider Ridge
Tern sub-basin
Pelican Fault
Hutton Fault
Alwyn Fault
10 km
PGS
c)
WNW
3/7-2
3/9a-1
3/9a-2
ESE
East Shetland Platform
West Margin Fault
Heather Fault
Ninian sub-basin
Ninian Fault
Alwyn Fault
BCU (U)
Top Brent Gp. (B)
Top Dunlin Gp. (D)
Top Statfjord Fm. (S)
Top Lunde Fm. (L)
Top Teist Fm. (T)
Pre-Triassic 3 (3)
Pre-Triassic 2 (2)
Pre-Triassic 1 (1)
Fault
10 km
PGS

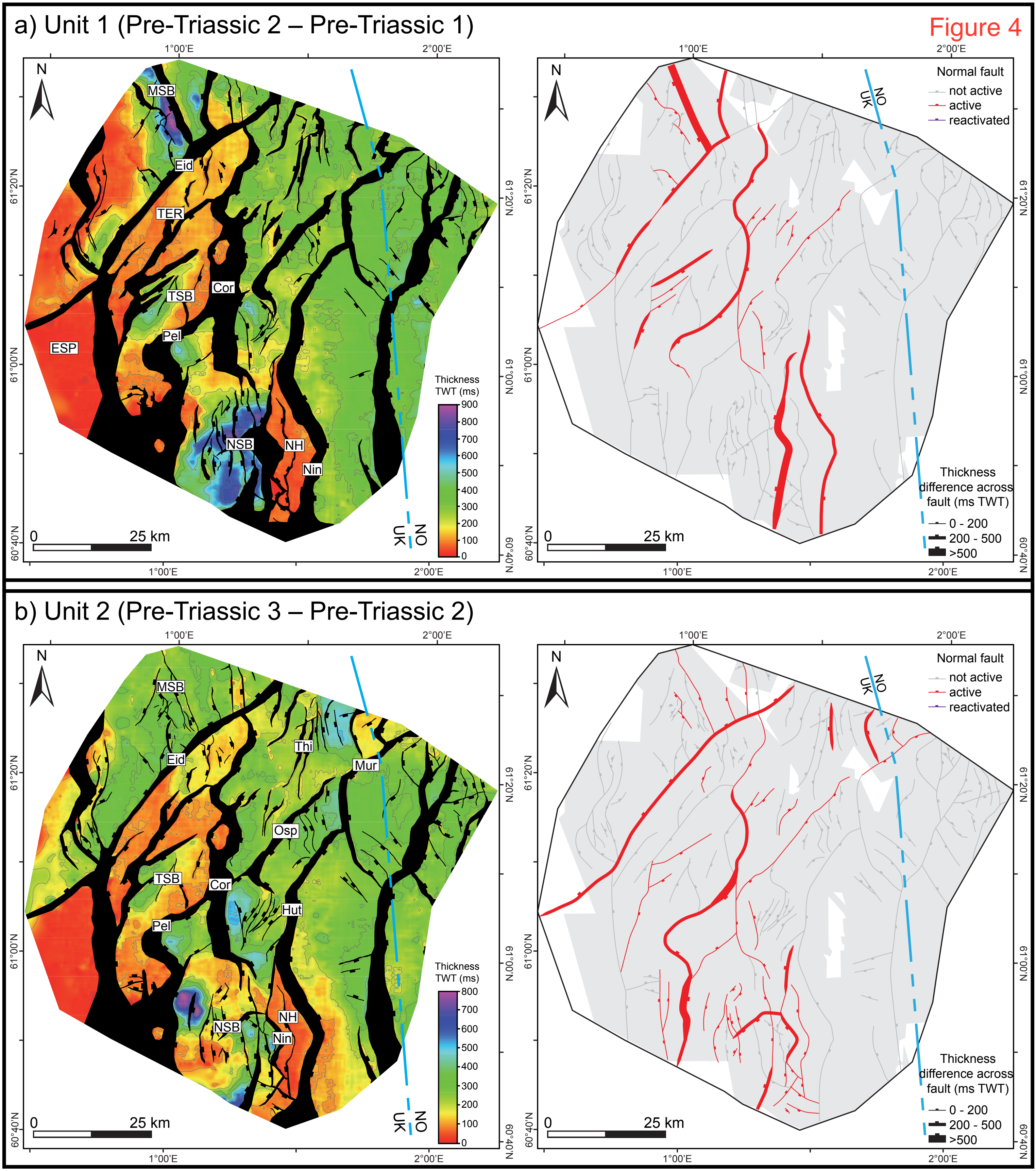

Figure 4
a) Unit 1 (Pre-Triassic 2 – Pre-Triassic 1)
b) Unit 2 (Pre-Triassic 3 – Pre-Triassic 2)
1°00'E
2°00'E
61°20'N
61°00'N
60°40'N
N
MSB
Eid
TER
TSB
Cor
Pel
ESP
NSB
NH
Nin
Thi
Mur
Osp
Hut
NO
UK
Thickness
TWT (ms)
0
100
200
300
400
500
600
700
800
900
0
25 km
Normal fault
not active
active
reactivated
Thickness
difference across
fault (ms TWT)
0 - 200
200 - 500
>500

Figure 4

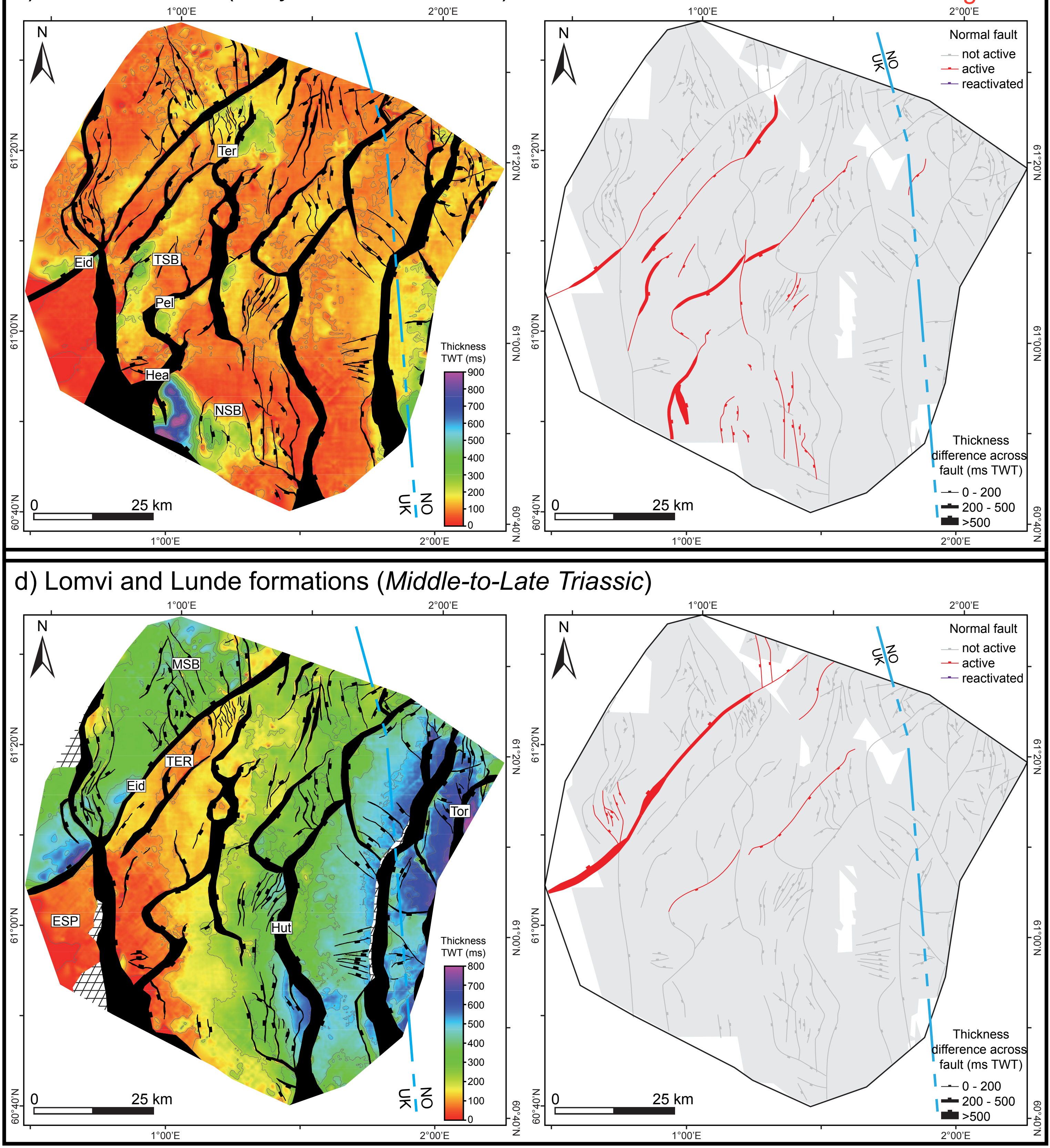
c) Teist Formation (Early-to-Middle Triassic)
N
1°00'E
2°00'E
61°20'N
61°00'N
60°40'N
Ter
Eid
TSB
Pel
Hea
NSB
Thickness
TWT (ms)
900
800
700
600
500
400
300
200
100
0
0
25 km
NO
UK
Normal fault
not active
active
reactivated
Thickness
difference across
fault (ms TWT)
0 - 200
200 - 500
>500
d) Lomvi and Lunde formations (Middle-to-Late Triassic)
MSB
TER
Eid
Tor
ESP
Hut
Thickness
TWT (ms)
800
700
600
500
400
300
200
100
0

Figure 4

e) Statfjord Formation (*Latest Triassic-to-Early Jurassic*)

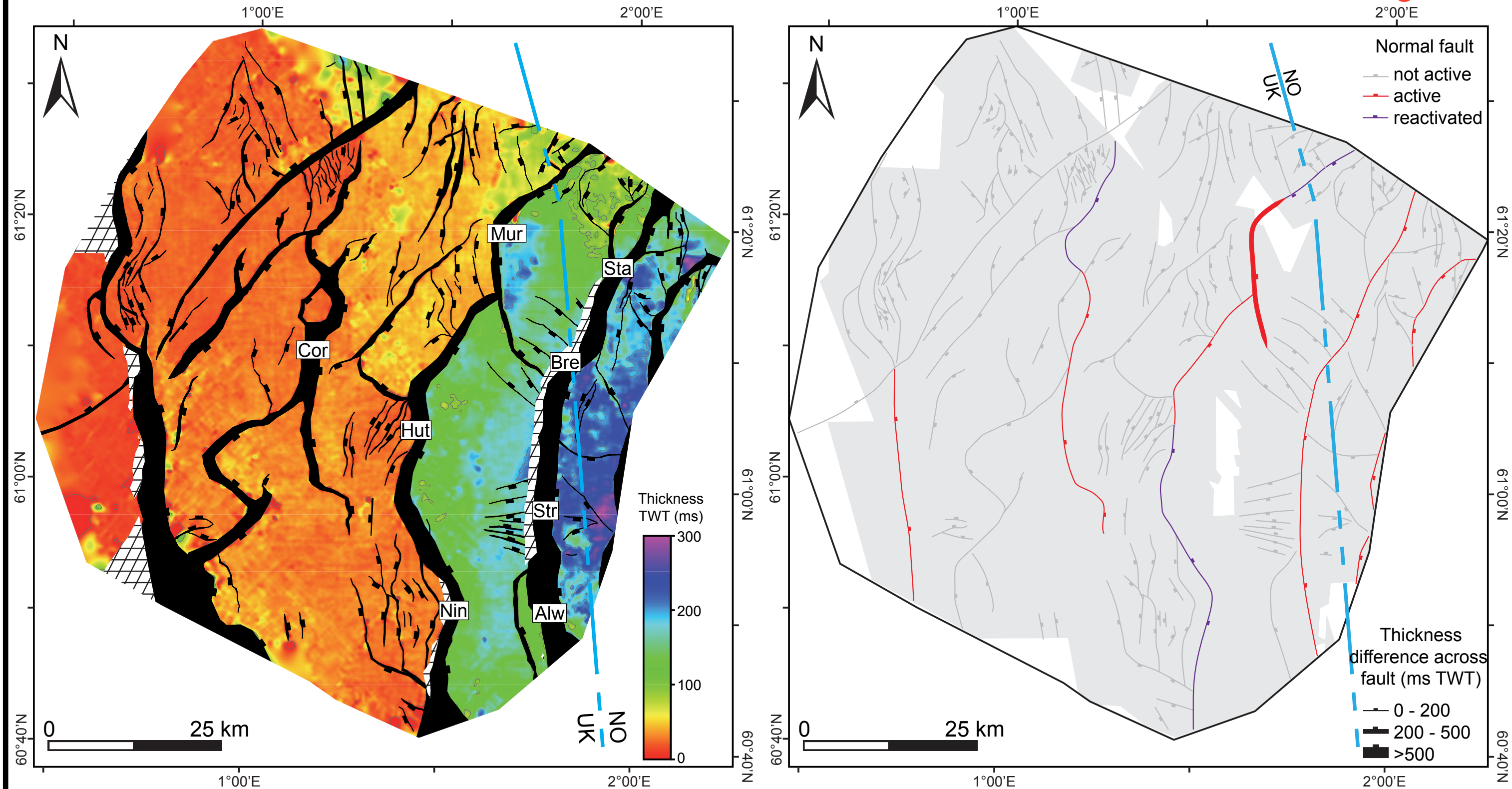

f) Dunlin Group (*Early Jurassic*)

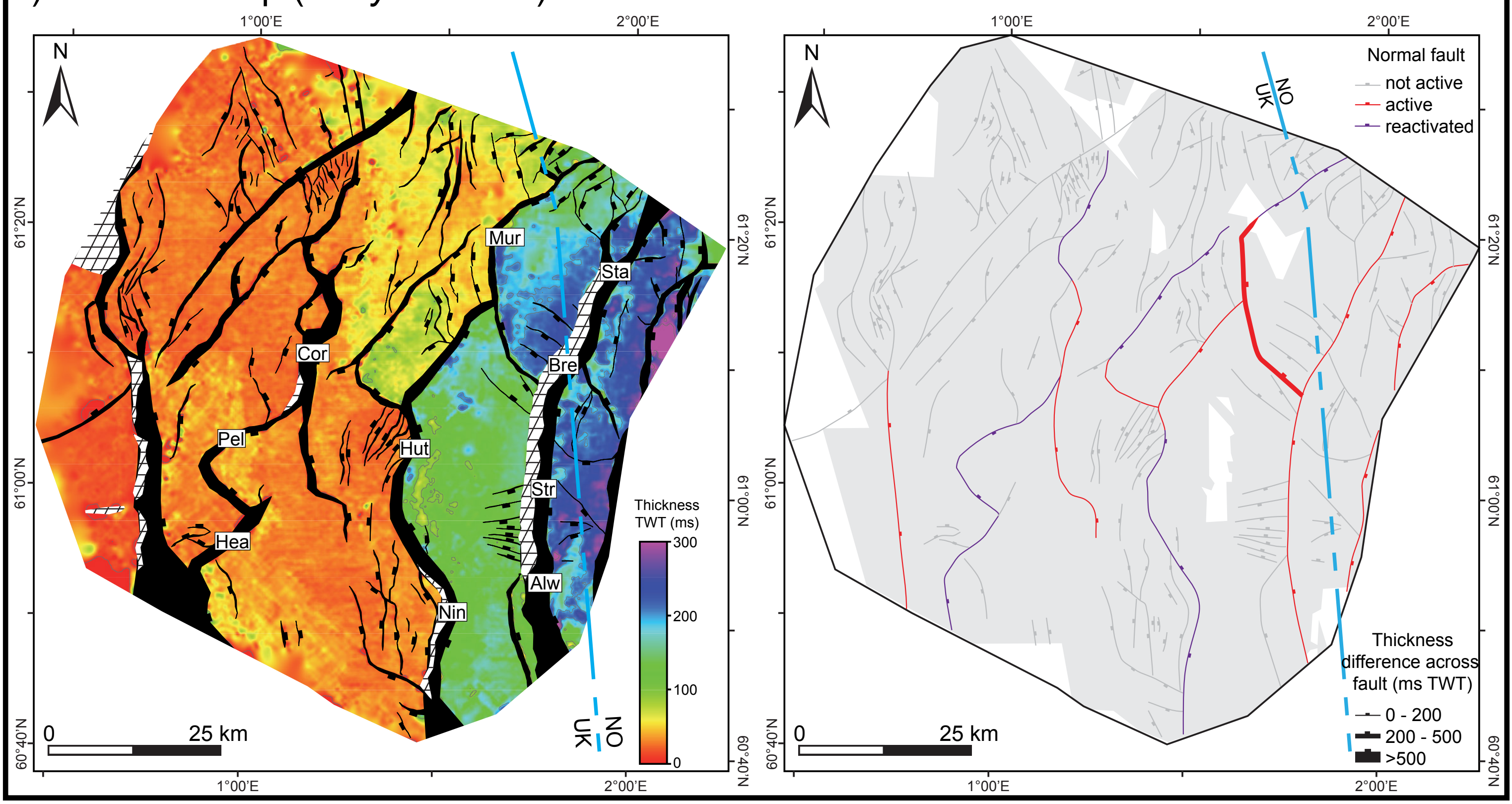

Figure 4

g) Brent Group (*Middle Jurassic*)

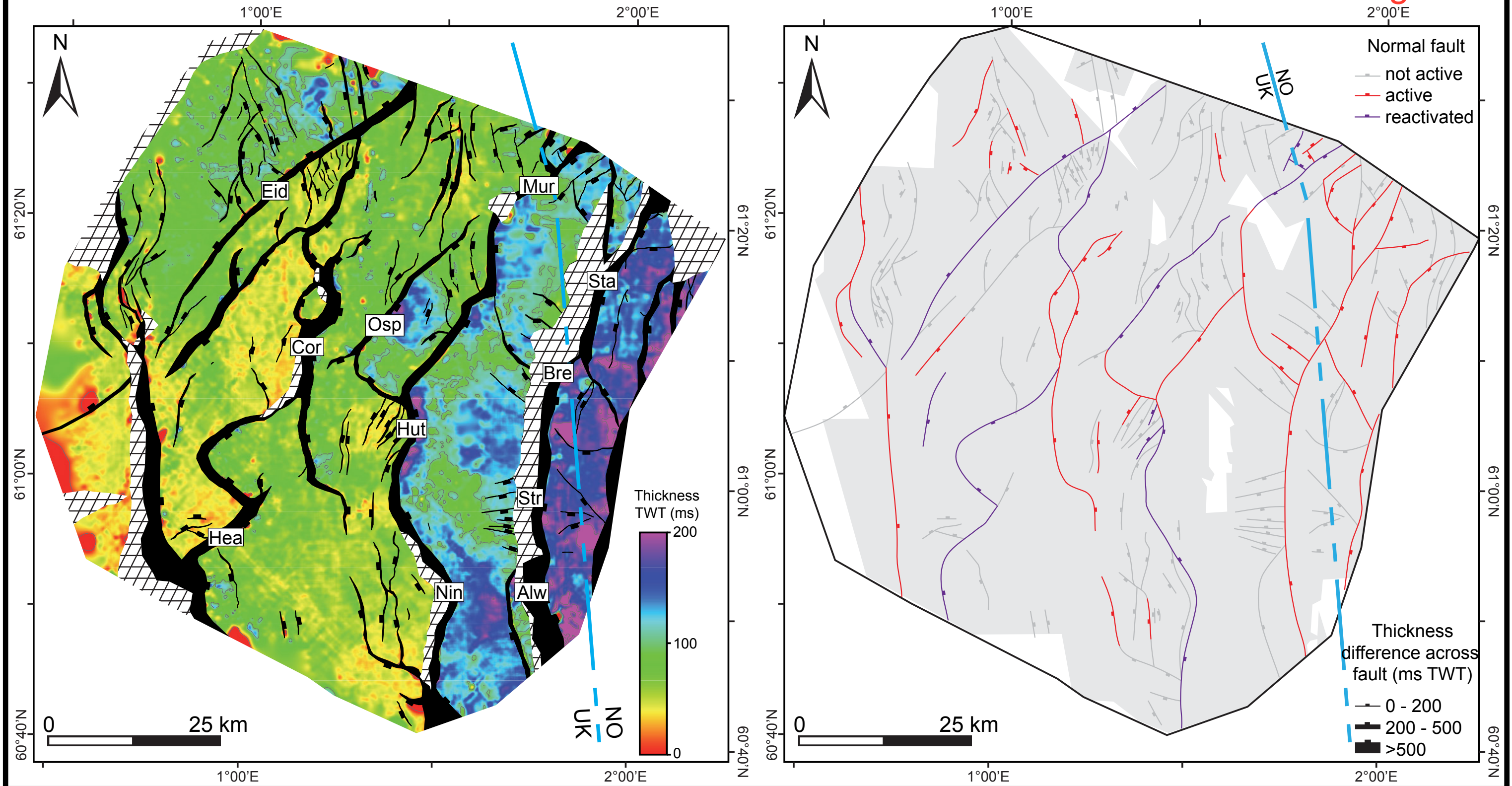

h) Viking Group (*Middle-to-Late Jurassic*)

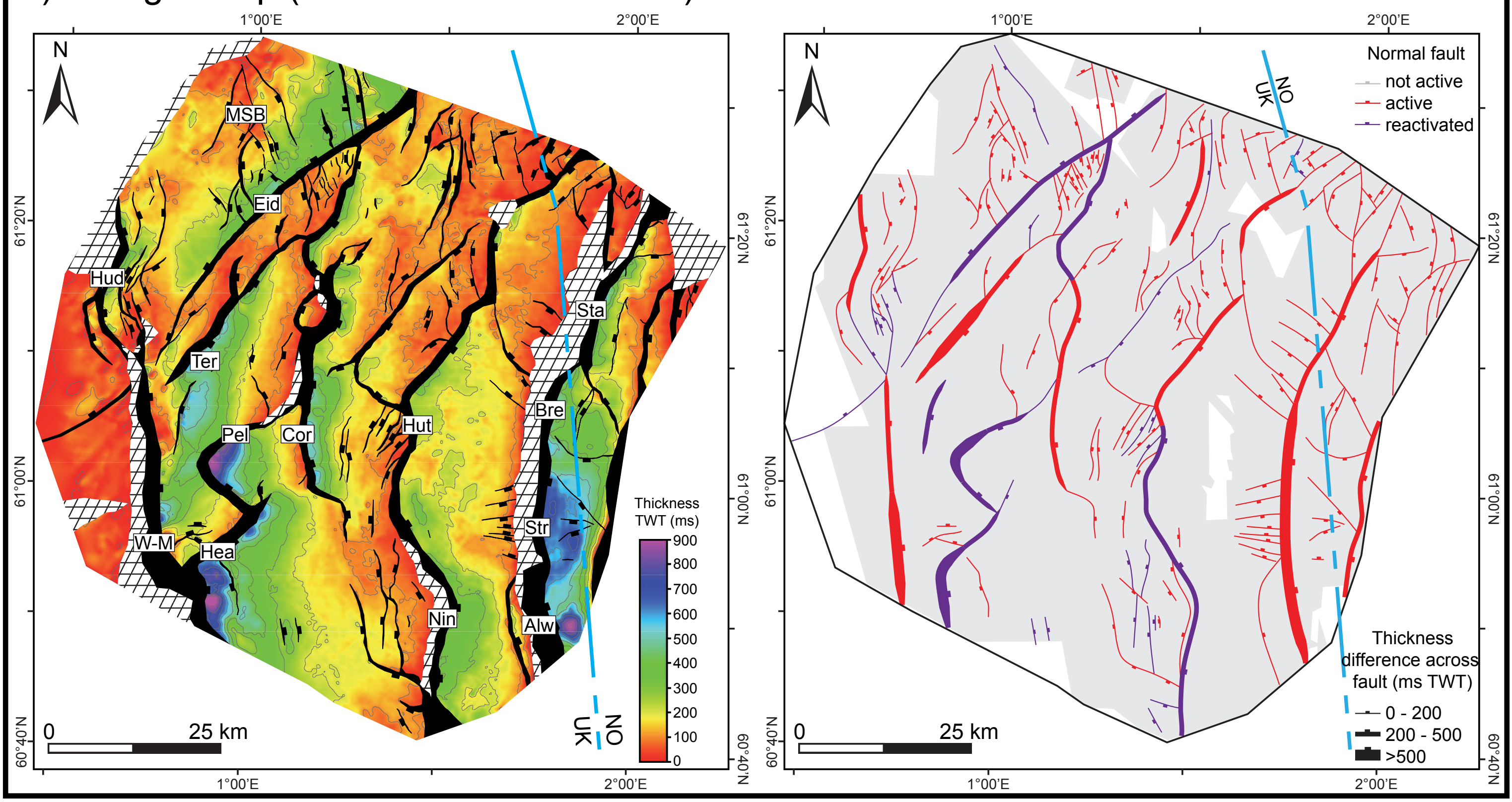

Figure 5

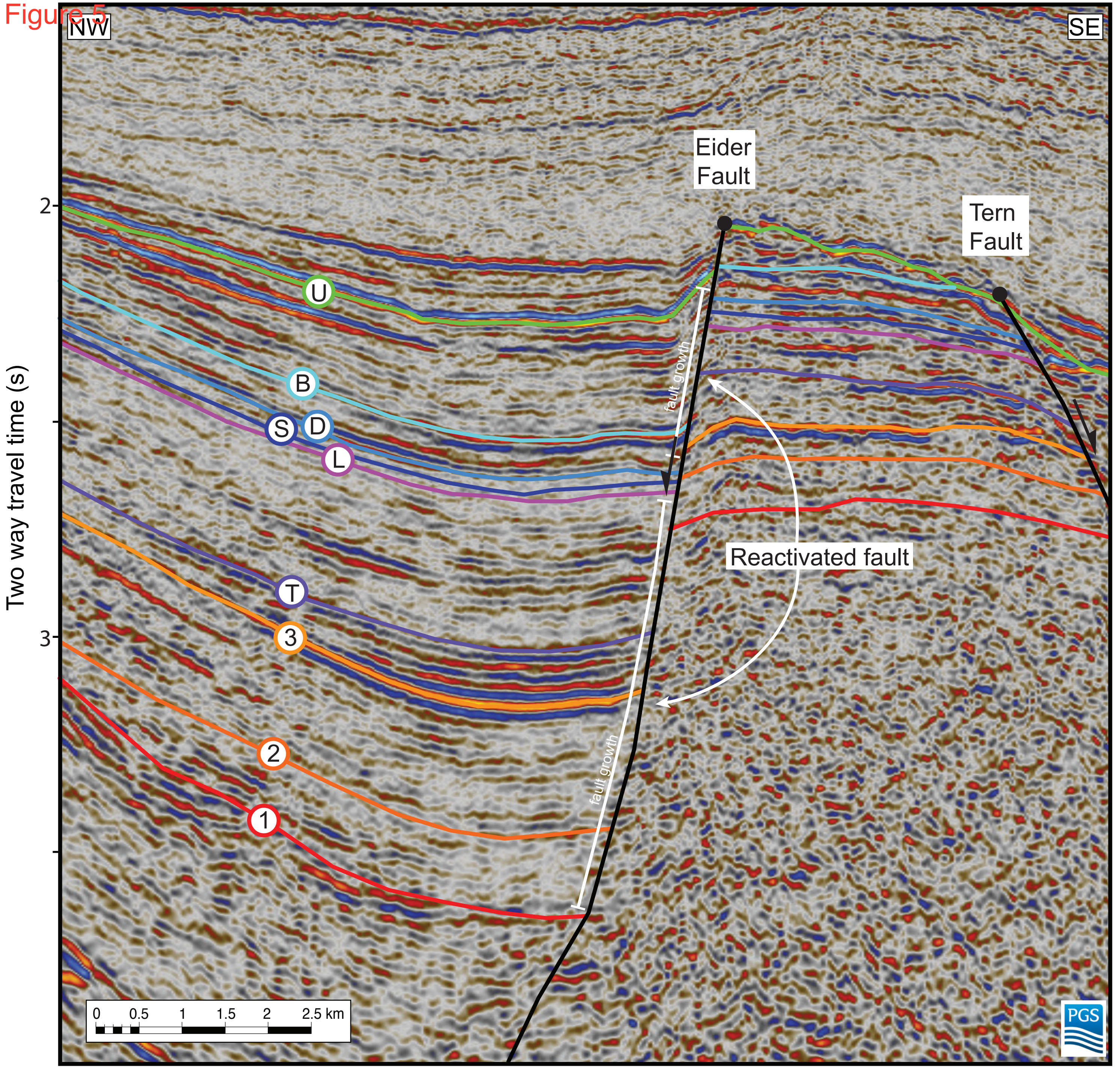
NW
SE
Eider Fault
Tern Fault
U
B
S
D
L
T
3
2
1
fault growth
fault growth
Reactivated fault
Two way travel time (s)
2
3
0
0.5
1
1.5
2
2.5 km
PGS

Figure 6

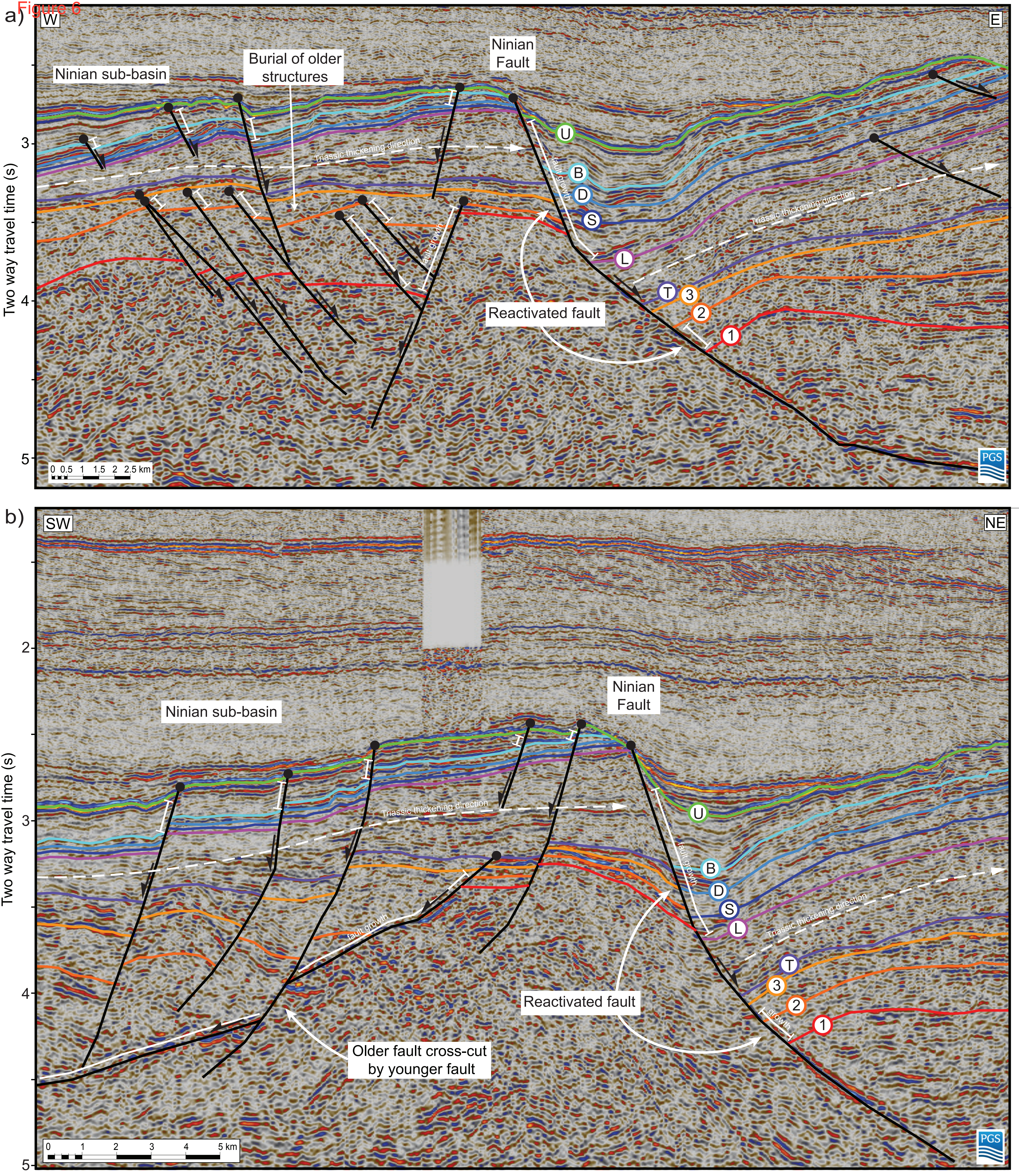
a)
W
E
Ninian sub-basin
Burial of older structures
Ninian Fault
Triassic thickening direction
fault growth
U
B
D
S
L
T
3
2
1
Reactivated fault
Two way travel time (s)
3
4
5
0 0.5 1 1.5 2 2.5 km
PGS
b)
SW
NE
2
3
4
5
Ninian sub-basin
Ninian Fault
Triassic thickening direction
fault growth
growth
Reactivated fault
Older fault cross-cut by younger fault
Two way travel time (s)
0 1 2 3 4 5 km
PGS

Figure 7

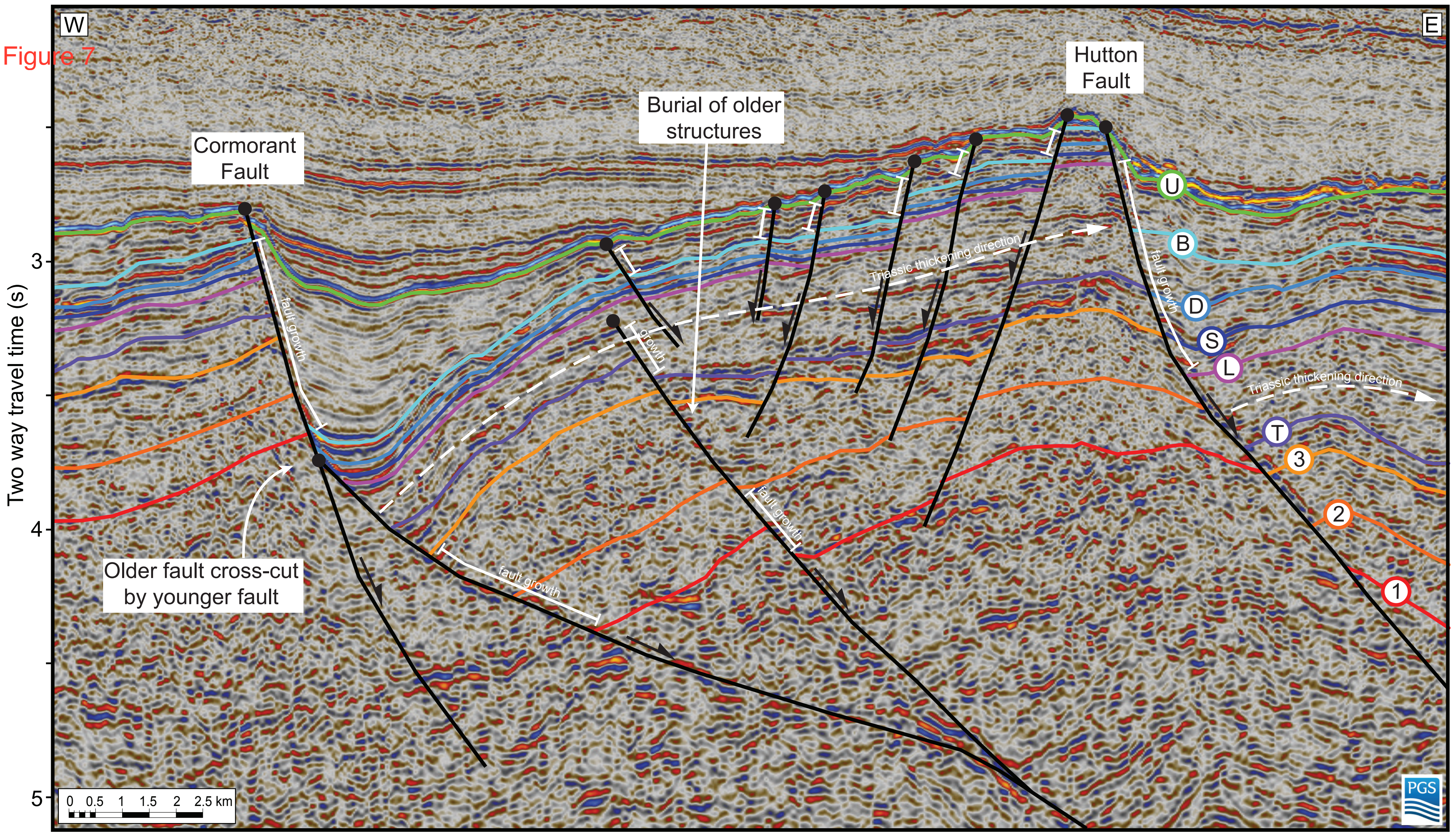

W
E
Hutton Fault
Burial of older structures
Cormorant Fault
U
B
D
S
L
T
3
2
1
Triassic thickening direction
Triassic thickening direction
fault growth
fault growth
fault growth
fault growth
growth
Older fault cross-cut by younger fault
Two way travel time (s)
3
4
5
0 0.5 1 1.5 2 2.5 km
PGS

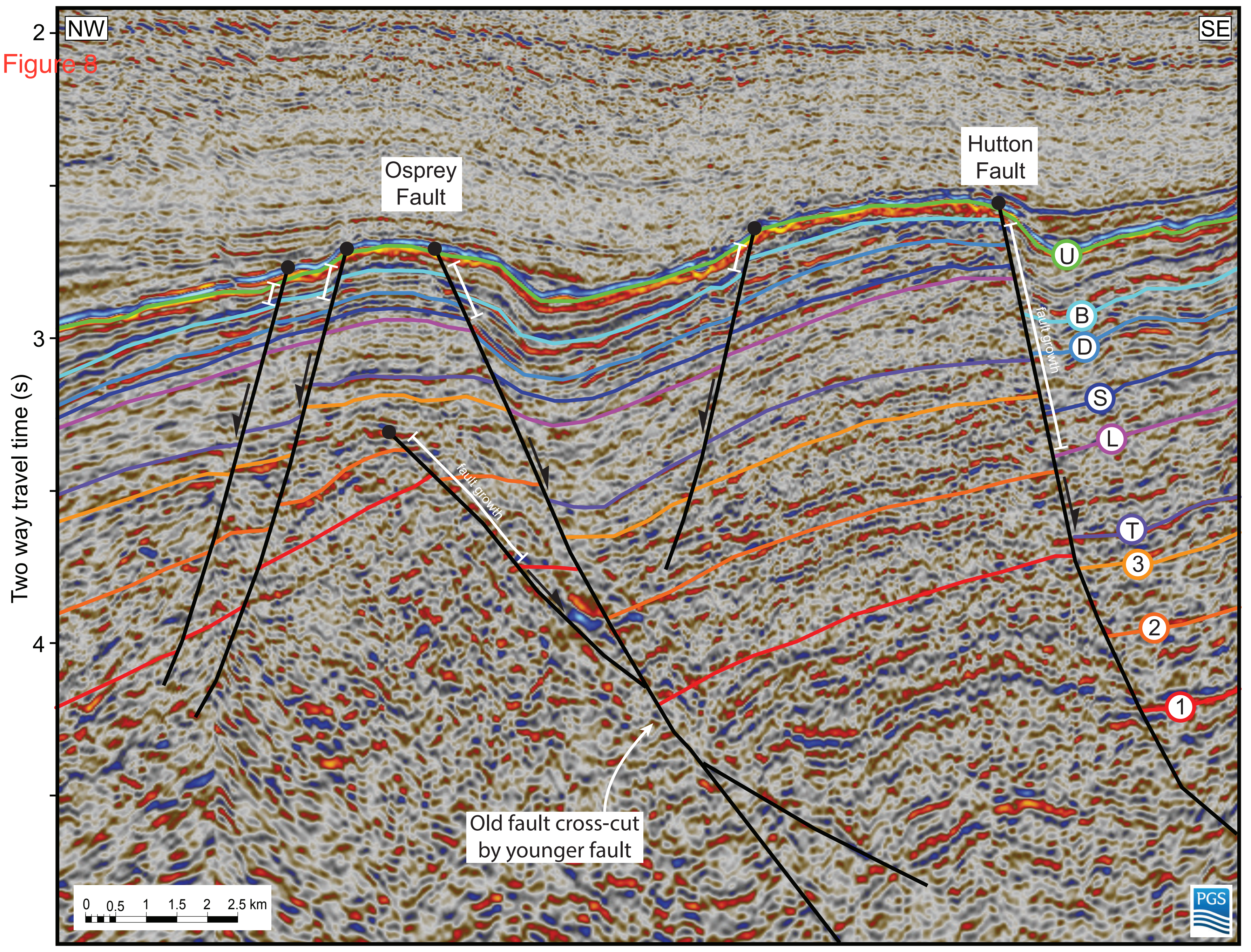

Figure 8
NW
SE
2
3
4
Two way travel time (s)
Osprey Fault
Hutton Fault
fault growth
fault growth
U
B
D
S
L
T
3
2
1
Old fault cross-cut by younger fault
0 0.5 1 1.5 2 2.5 km
PGS

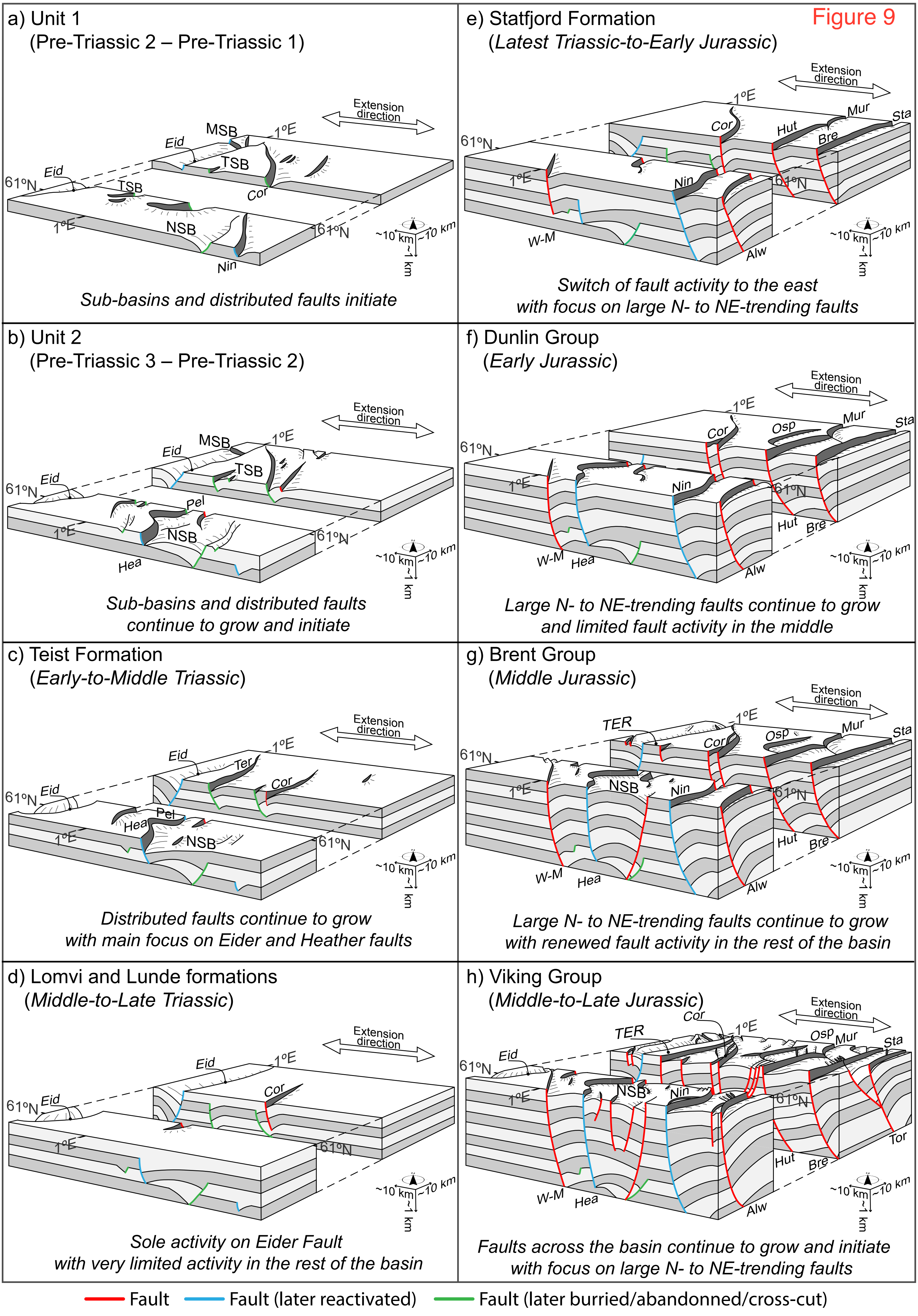
Figure 9
a) Unit 1
(Pre-Triassic 2 – Pre-Triassic 1)
Extension direction
MSB
Eid
TSB
Cor
NSB
Nin
61°N
1°E
~10 km
~10 km
~1 km
Sub-basins and distributed faults initiate
b) Unit 2
(Pre-Triassic 3 – Pre-Triassic 2)
Extension direction
MSB
Eid
TSB
Pel
NSB
Hea
61°N
1°E
Sub-basins and distributed faults
continue to grow and initiate
c) Teist Formation
(Early-to-Middle Triassic)
Extension direction
Eid
Ter
Cor
Hea
Pel
NSB
61°N
1°E
Distributed faults continue to grow
with main focus on Eider and Heather faults
d) Lomvi and Lunde formations
(Middle-to-Late Triassic)
Extension direction
Eid
Cor
61°N
1°E
Sole activity on Eider Fault
with very limited activity in the rest of the basin
e) Statfjord Formation
(Latest Triassic-to-Early Jurassic)
Extension direction
Cor
Hut
Mur
Bre
Sta
Nin
W-M
Alw
61°N
1°E
Switch of fault activity to the east
with focus on large N- to NE-trending faults
f) Dunlin Group
(Early Jurassic)
Extension direction
Cor
Osp
Mur
Sta
Nin
Hut
Bre
W-M
Hea
Alw
61°N
1°E
Large N- to NE-trending faults continue to grow
and limited fault activity in the middle
g) Brent Group
(Middle Jurassic)
Extension direction
TER
Cor
Osp
Mur
Sta
NSB
Nin
Hut
Bre
W-M
Hea
Alw
61°N
1°E
Large N- to NE-trending faults continue to grow
with renewed fault activity in the rest of the basin
h) Viking Group
(Middle-to-Late Jurassic)
Extension direction
Cor
TER
Osp
Mur
Sta
Eid
NSB
Nin
Tor
Hut
Bre
W-M
Hea
Alw
61°N
1°E
Faults across the basin continue to grow and initiate
with focus on large N- to NE-trending faults
Fault
Fault (later reactivated)
Fault (later burried/abandonned/cross-cut)

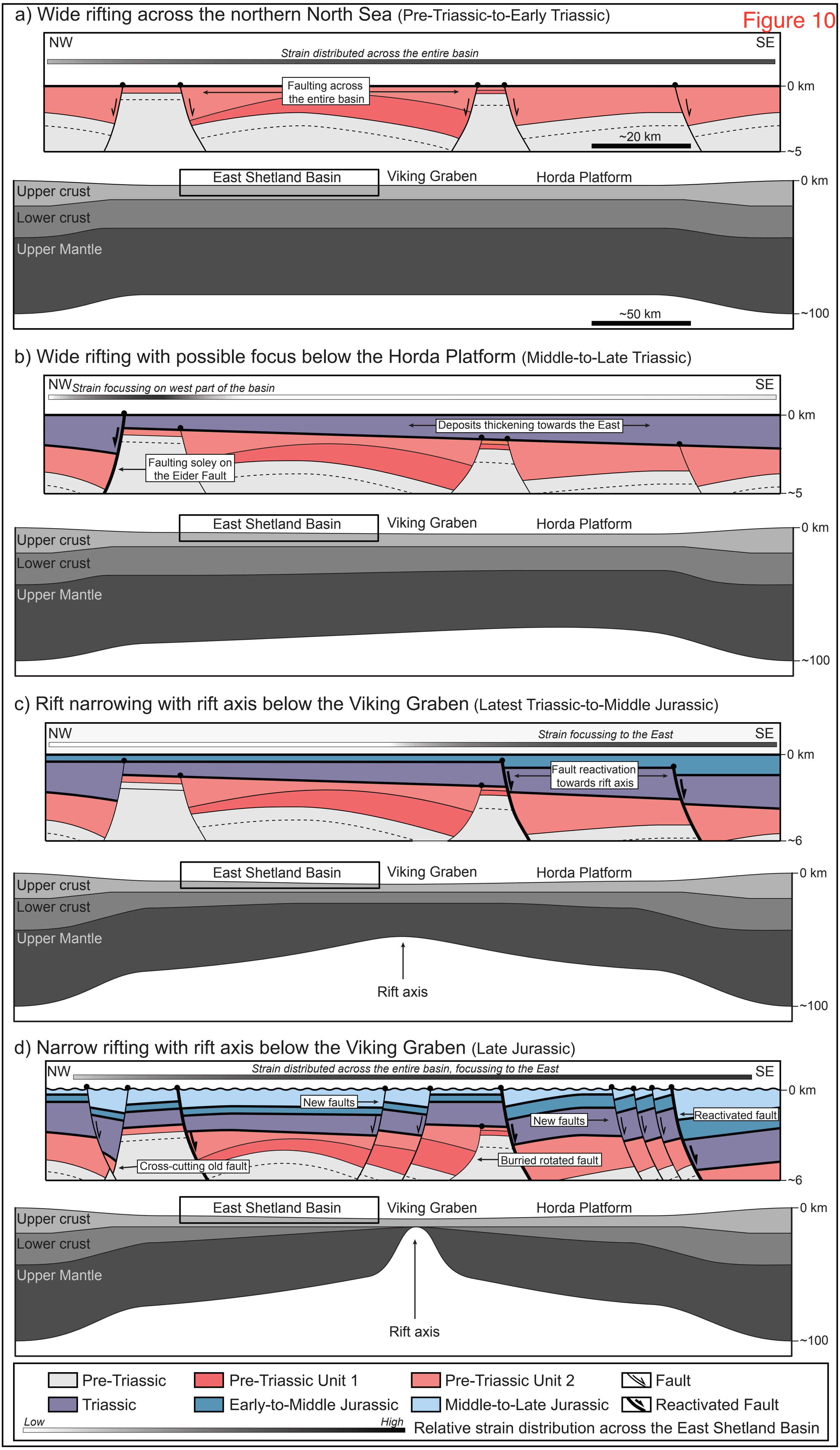

Figure 10
a) Wide rifting across the northern North Sea (Pre-Triassic-to-Early Triassic)
NW
SE
Strain distributed across the entire basin
Faulting across the entire basin
0 km
~20 km
~5
East Shetland Basin
Viking Graben
Horda Platform
0 km
Upper crust
Lower crust
Upper Mantle
~50 km
~100
b) Wide rifting with possible focus below the Horda Platform (Middle-to-Late Triassic)
NW
Strain focussing on west part of the basin
SE
0 km
Deposits thickening towards the East
Faulting soley on the Eider Fault
~5
East Shetland Basin
Viking Graben
Horda Platform
0 km
Upper crust
Lower crust
Upper Mantle
~100
c) Rift narrowing with rift axis below the Viking Graben (Latest Triassic-to-Middle Jurassic)
NW
Strain focussing to the East
SE
0 km
Fault reactivation towards rift axis
~6
East Shetland Basin
Viking Graben
Horda Platform
0 km
Upper crust
Lower crust
Upper Mantle
Rift axis
~100
d) Narrow rifting with rift axis below the Viking Graben (Late Jurassic)
NW
Strain distributed across the entire basin, focussing to the East
SE
0 km
New faults
New faults
Reactivated fault
Burried rotated fault
Cross-cutting old fault
~6
East Shetland Basin
Viking Graben
Horda Platform
0 km
Upper crust
Lower crust
Upper Mantle
Rift axis
~100
Pre-Triassic
Pre-Triassic Unit 1
Pre-Triassic Unit 2
Fault
Triassic
Early-to-Middle Jurassic
Middle-to-Late Jurassic
Reactivated Fault
Low
High
Relative strain distribution across the East Shetland Basin